NASA TECHNICAL NOTE

NASA TN D-4821

NASA TN D-4821

EFFECT ON BASE DRAG OF RECESSING THE BASES OF CONICAL AFTERBODIES AT SUBSONIC AND TRANSONIC SPEEDS

by William B. Compton III

Langley Research Center
Langley Station, Hampton, Va.

NATIONAL AERONAUTICS AND SPACE ADMINISTRATION • WASHINGTON, D. C. • OCTOBER 1968

EFFECT ON BASE DRAG OF RECESSING THE BASES OF CONICAL AFTERBODIES AT SUBSONIC AND TRANSONIC SPEEDS

By William B. Compton III

Langley Research Center
Langley Station, Hampton, Va.

NATIONAL AERONAUTICS AND SPACE ADM~~INISTRATION~~

For sale by the Clearinghouse for Federal Scientific and Technical Information
Springfield, Virginia 22151 – CFSTI price $3.00

EFFECT ON BASE DRAG OF RECESSING THE BASES OF CONICAL AFTERBODIES AT SUBSONIC AND TRANSONIC SPEEDS

By William B. Compton III
Langley Research Center

SUMMARY

An investigation has been conducted to determine the effect on base drag of recessing the bases of truncated conical afterbodies. The drag of a flat base was compared with the drag of recessed bases of equal size for afterbodies having boattail angles of 0°, 3°, 5°, and 10°, and having ratios of boattail length to maximum diameter of 1.0 and 1.5. For each boattail, the amount of base concavity was varied in several steps from a flat base to an open base. A fully conical afterbody with a boattail angle of 10° was tested also. The tests were run at an angle of attack of 0° and through a Mach number range of 0.3 to 1.3. The Reynolds number based on model length was in the range of 8×10^{6} to 16×10^{6} depending on the Mach number.

In addition to the base-drag information, boundary-layer profiles and afterbody-drag-coefficient plots are included. Results indicate that, in general, recessing the base gives an increase in base pressure coefficient of 0.01 to 0.03, depending on the boattail, and hence a reduction in base drag. For a given boattail, base drag decreases with increasing base concavity up to a certain point, but, beyond this point, further concaving the base has little or no effect. The ratio of the amount of base concavity to base radius necessary to achieve maximum base-drag reduction depends on the boattail angle and length. Recessing the base has practically no effect on boattail drag.

INTRODUCTION

The base drag of an aircraft, unpowered projectile, or missile with a blunt base can represent a large portion of the total drag; and the effectiveness of ways of reducing this drag has been the objective of many investigations. Considerable work has been done on the reduction of base drag by the base-bleed and splitter-plate methods (e.g., see refs. 1 and 2). One method of interest, on which a lesser amount of work has been done, particularly for axisymmetric flow, is recessing the base. The present work is a corollary to that reported in references 3, 4, and 5, which were concerned with pressure recovery on recessed bases of bodies immersed in jet flow.

This investigation was conducted to determine the effects on base drag of recessing the bases of axisymmetric bodies having truncated conical boattails. These effects were investigated on a cone-cylinder nacelle having afterbodies with boattail angles of 0°, 3°, 5°, and 10° and with ratios of boattail length to maximum diameter of 1.0 and 1.5. For each boattail, the amount of base concavity was varied in several steps from a flat base to an open base. The afterbody drag of a fully conical afterbody with a boattail angle of 10° was measured also to determine the drag penalty incurred in truncating a cone. In addition to the base-drag information, boundary-layer profiles and afterbody-drag-coefficient plots are presented. Boundary-layer transition was fixed at a point 5.08 centimeters from the nose of the model.

The investigation was conducted at the Langley 16-foot transonic tunnel through a Mach number range of 0.3 to 1.3 and at an angle of attack of 0°. The Reynolds number based on model length was in the range of 8×10^6 to 16×10^6 depending on the Mach number.

SYMBOLS

A	area, square meters
B	station at junction of cylindrical section of model and boattail (see figs. 4 and 5), meters
C_D	drag coefficient based on maximum cross-sectional area of model
C_p	pressure coefficient
$\Delta C_{p,b}$	incremental base pressure coefficient (average base pressure coefficient for concave base minus average base pressure coefficient for flat base)
c	base concavity (depth of base cavity parallel to center line of model), meters
D_m	maximum diameter of model (see figs. 1, 4, and 5), 0.1524 meter
d	diameter of center section of semitoroidal concave base (see fig. 5), 0.0030 meter
E	station at end of model, meters
F_A	force acting on model in axial direction, drag positive, newtons

L	length of boattail parallel to boattail surface, meters
M	free-stream Mach number
M_l	local Mach number
p	pressure, newtons per square meter
q	free-stream dynamic pressure, newtons per square meter
R	radius, meters
r	radial distance from axis of symmetry of model (see fig. 5), meters
V_l	local velocity, meters per second
V_δ	velocity at edge of boundary layer, meters per second
x	axial distance from station B measured parallel to axis of symmetry of model, rearward direction positive (see fig. 4), meters
y	radial distance from model surface (see fig. 1), meters
α	divergence angle on inside of open-base configurations (see fig. 5), degrees
β	boattail angle (angle between axis of symmetry and a generatrix of model afterbody), degrees
δ	thickness of boundary layer, meters
ϕ	angular location measured from, and in a plane perpendicular to, axis of symmetry of model, clockwise direction positive when viewed from rear with 0° at top of model (see figs. 1 and 5), degrees

Subscripts:

a	afterbody

b	base
bal	computed from balance measurement (total)
f	skin friction
gap	gap in model shell just aft of junction of nose and cylindrical section of model (see fig. 4)
i	integer
m	maximum
β	boattail
1,2	pertains to particular radii of the base geometry (see fig. 5)
∞	free stream

APPARATUS AND PROCEDURE

Wind Tunnel

This investigation was conducted in the Langley 16-foot transonic tunnel, which is a single-return, continuous tunnel with an octagonal slotted test section measuring 4.73 meters across the flats. By pumping low-energy air from the plenum which surrounds the slotted test section, a Mach number of 1.3 can be attained. For cooling, the tunnel is equipped with an air-exchange tower which continuously exchanges air with the atmosphere, the result being that the tunnel stagnation pressure is approximately equal to atmospheric pressure.

Model

The basic model to which the different afterbody configurations were attached was a cone-cylinder nacelle with a rounded shoulder at the junction of the nose and cylindrical section (see fig. 1). Boundary-layer transition was fixed at 5.08 centimeters from the nose of the model by a strip of no. 100 grit approximately 5 millimeters wide. The model was supported from the tunnel floor by a 5-percent-thick strut swept back with respect to the model and having a leading-edge sweep of 45°.

Figure 1 shows the geometry of the model and strut as used to survey the boundary layer and the pressures along a cylindrical afterbody. Three boundary-layer rakes were attached 45° apart to a removable section of the model so that they could be indexed to record data at $\phi = 0^{\circ}$, 45°, and 90° or at $\phi = 90^{\circ}$, 135°, and 180°. The afterbody pressure orifices were measured axially from station 104.14 with the rearward direction positive. The locations of the orifices pertinent to this part of the investigation are given in figure 1. Figure 2 is a photograph of the model with boundary-layer rakes installed, and figure 3 gives the area distribution of the model and support strut.

The geometry of the model pertinent to the investigation of the effects of recessing the base is shown in figure 4. The model was designed as an air-powered jet nacelle, but inasmuch as the jet was not used in this investigation, the details of the air system are not shown. A three-component balance supported and sensed forces on the entire shell of the model aft of the gap. Configuration geometry was varied only aft of station B, the junction of the cylindrical section and the boattail. This junction was a nominally sharp corner.

The geometry of the different afterbody configurations used in the investigation of the effects of recessing the base is shown in figure 5. Boattails with angles of 0°, 3°, 5°, and 10° and with ratios of length to maximum diameter of 1.0 and 1.5 were investigated. For each boattail, the bases were recessed in several steps from a flat to an open base. On two boattails ($\beta = 5^{\circ}$ for L/D_m of 1.0 and 1.5), semitoroidal concave bases (ref. 5) of $c/R_b = 0.50$ were tested in addition to the simply concaved bases. A fully conical afterbody with boattail angle of 10° was tested also.

Since it was desirable to keep the model as nearly the same length as possible for each configuration, station B had two locations, one for each boattail length. As a result, all the configurations except one were within 4 millimeters of the same length. The one exception was the fully conical afterbody, which was approximately 17 centimeters longer (see fig. 5).

The outermost part of the cavity at the base of the concave bases was made parallel to the boattail (see base-geometry sketches in fig. 5). Thus, the rims of the concave bases were flat; however, the rim width was kept as small as possible. The width is shown by the difference in R_1 and R_b in figure 5. No attempt was made to measure the pressure on the rims of the concave bases. As shown in figure 5, different bases were inserted into the boattails, so, of necessity, the outermost part of the cavity of the open-base configurations could not be kept parallel to the boattail.

For the configurations used in the investigation of the effects of recessing the base, the location of the pressure orifices on the surface of the boattail was measured axially from station B, and the location of those on the base was measured radially from the model axis. The locations of the orifices for these configurations are given in tables 1 and 2. The base orifices for the open-base configurations were located well within the model and were not purposely placed at any special radial location since their exact placement was relatively unimportant.

Figures 6 and 7 show photographs of the assembled model and of each type base.

Instrumentation and Tests

Pressures were measured on the base, on the boattail surface, and in the model-shell gap with strain-gage pressure transducers. The forces and moments on that portion of the model aft of the gap were measured by an internal strain-gage balance.

The tests were conducted at 0° angle of attack and through a Mach number range of 0.3 to 1.3. For each run, data were taken at specific Mach numbers as Mach number was increased, and repeat points were taken as Mach number was lowered. As each point of data was taken, the Mach number was held constant. The points taken as Mach number was decreased are identified in the plots by flagged symbols. For each data point, approximately five frames of data were recorded within 1 second and the average was used to compute the values of force, pressure, and so forth.

Data Reduction

The main drag coefficients of concern in the report are the base drag coefficient $C_{D,b}$, afterbody pressure-drag coefficient $C_{D,a}$, and total afterbody drag coefficient $C_{D,a,bal}$, with the afterbody defined as the entire model aft of the junction of the cylindrical section and the boattail (station B). As explained subsequently, the base drag was computed by pressure integration, whereas the afterbody drag was computed both by pressure integration, giving afterbody pressure drag, and from balance data, giving total afterbody drag.

Base drag and afterbody pressure drag were obtained by assigning an incremental area to each pressure orifice at $\phi = 0^{\circ}$ and integrating. Skin-friction drag was not included in the afterbody pressure drag. All drag coefficients are based on the maximum cross-sectional area of the model. The equation for pressure-drag coefficient is

$$C_D = \frac{1}{qA_m} \sum_{i=1}^{n} \left(p_{\infty} - p_i\right) A_i$$

For the base drag integration, the area assigned to the outermost orifice extended to the full radius of the base $\left(R_b\right)$. Thus, the value of integrated base drag for the concave bases approached the value that would be obtained for $R_1 = R_b$ (see fig. 5).

The incremental base pressure coefficients, used in comparing the average base pressures of all configurations, were calculated by using the following formula for each boattail:

$$\Delta C_{p,b_i} = \left(C_{D,\text{flat base}} - C_{D,\text{concave base}_i}\right)\frac{A_m}{A_b} \quad (\text{where} \quad i = 1 \ldots n)$$

The balance measured the total force on the model from the gap aft. To obtain total afterbody drag from the balance, the force measured by the balance was corrected for gap force and skin-friction drag between the gap and the break of the boattail (station B). The skin-friction-drag calculation was based on turbulent-boundary-layer theory. The total afterbody drag coefficient was calculated from the balance as follows:

$$C_{D,a,bal} = \frac{1}{qA_m}\left[F_{A,bal} - \sum_{i=1}^{n}\left(p_{i,gap} - p_\infty\right)A_{i,gap} - F_{A,f}\right]$$

In this equation $F_{A,f}$ is the calculated skin-friction force between the gap and station B. Thus the total afterbody drag computed from the balance measurement includes the effect of skin friction on the boattail and of asymmetry of pressures with ϕ, whereas the integrated afterbody pressure drag did not.

RESULTS AND DISCUSSION

Cylindrical Afterbody Pressures and Boundary-Layer Profiles

Figure 8 shows the boattail-surface-pressure-coefficient distribution on a cylindrical afterbody with a flat base for various Mach numbers and values of ϕ, $x/D_m = 0$ being located at model station 104.14 (station B for an afterbody with $L/D_m = 1.0$). (See fig. 1.) The general drop in pressure over the whole boattail at the subsonic Mach numbers is due to expansion of the flow at the base. At the supersonic Mach numbers, where the base effects do not feed as far upstream, the pressures over most of the boattail are almost constant. These same trends are evident for the models used in reference 6. At most Mach numbers, the pressures of the different rows of orifices are about equal except near the base where the pressures of the bottom row (at $\phi = 180^\circ$) are generally lower, an effect possibly caused by the strut wake. Between, but not including, Mach numbers 0.95 and 1.20, normal and reflected shocks, influenced by the support strut, on the model or near its base cast doubt on the correct level of pressures on the boattail.

Boundary-layer Mach number profiles for various free-stream Mach numbers are presented in figure 9. Since the boundary-layer rakes measured only total pressure, the static pressure in the boundary layer was assumed constant in calculating the Mach number profiles. The value used was equal to the static pressures on the model in the position of the rakes with the rakes removed. The profiles show the boundary layer to be about 1.52 centimeters thick ($y/D_m = 0.1$) and very consistent at all values of ϕ

except 180°, where there is a loss of total pressure in the wake of the model support strut. The experimental and power-law-calculated boundary-layer profiles are compared in figure 10 for a representative subsonic and supersonic Mach number. To calculate the ratio of the local to maximum boundary-layer velocity, the total temperature throughout the boundary layer was assumed constant. The boundary-layer displacement thickness is approximately one-tenth of the boundary-layer thickness and eleven-hundredths of the maximum diameter of the model.

Variation of Pressures With ϕ and Base Concavity

Figures 11 and 12 illustrate the reason for using the top row of orifices (at $\phi = 0^\circ$) for pressure integration. Figure 11 shows typical boattail-pressure-coefficient distributions at various Mach numbers and values of ϕ. The boattail-pressure levels of the different rows of orifices are practically the same except at a Mach number of 1.30, where the bottom row is at a higher pressure level than the others. Figure 12 shows typical base-pressure-coefficient distributions at various Mach numbers and values of ϕ. The base-pressure levels also vary with ϕ, particularly at Mach numbers of 0.80 and 1.30. This variation of pressure with ϕ is thought to be caused by the flow disturbance of the model support strut, and hence the top row of pressure orifices should be the most interference free. Therefore, only the top row was used when integrating the base and boattail pressures for drag.

Typical boattail-pressure-coefficient distributions for various Mach numbers and values of base concavity are shown in figure 13. This figure indicates that any effect of recessing the base on boattail pressures is practically nil; thus, the effect of base concavity is confined to the base.

Base Drag and Pressures

Figures 14 and 15 show the effect of concaving the base on base pressures, and hence base drag. Figure 14 presents the radial distribution of base pressure coefficient, with the abscissa being the ratio of radial location on the base to maximum model radius. Results for each configuration are plotted, in groups of bases relating to each boattail, at Mach numbers of 0.40, 0.80, 0.90, and 1.30. Since the exact radial location of the base orifices for the open-base configurations was relatively unimportant, the averages of the pressure coefficients of these orifices are plotted at $r/R_m = 1.0$ and the symbols are solid.

Figure 15 is a plot of base drag coefficient as a function of Mach number for each configuration. The ratio of the base area to maximum cross-sectional area of the model is given for each boattail so that the relative size of the bases can be taken into account when comparing the effects of recessing the bases of the different boattails. Because of normal and reflected shocks on the model and near the base between Mach numbers 0.95 and 1.20, the data in this Mach number range were not faired.

Figures 14 and 15 show generally that recessing the base gives a reduction in base drag at both subsonic and transonic speeds. As can be seen from figure 14, the maximum base-pressure-coefficient benefits derived from recessing the base varied from 0.01 to 0.03 depending on the boattail. Although not directly shown or discussed in reference 7, a comparison of figures 3 and 9 in that reference would show the same results were obtained with a turbulent boundary layer. When the base of the model in reference 7 was concaved by fitting it with a cylindrical tube having the same diameter as the model and a length approximately equal to its diameter, and having thin, solid walls, the base pressure coefficient was increased by approximately 0.02.

To better illustrate the effect of varying the depth of base cavity, figure 15 is summarized in figure 16 for a representative subsonic and transonic Mach number. The change in base pressure coefficient derived from concaving the base is plotted for each boattail, with the abscissa being the ratio of base concavity to base radius. The incremental base pressure coefficients, plotted as the ordinate, were obtained for each boattail by subtracting the drag coefficients of the concave bases from the drag coefficient of the flat base and multiplying by the ratio of the maximum area of the model to the base area.

Figure 16 shows that, in general, for a given boattail angle and length, base pressure increases with increasing base concavity up to a particular ratio of base concavity to base radius, but, beyond this ratio, further concaving the base has little or no effect. This result is particularly true at the subsonic Mach numbers. It also appears that, in general, the steeper boattail angles require a greater ratio of base concavity to base radius to derive the maximum base-pressure benefits from recessing the base than do the shallower boattail angles. Again this effect is more evident at the subsonic Mach numbers.

As seen from figure 15, at a boattail angle of 5°, for a depth of base cavity of one-half the base radius, and through the test Mach number range, the semitoroidally concaved base offered no improvement over the base simply concaved to the same depth. The pressures for the two types of bases are presented in figures 14(b) and 14(f). The semitoroidally concaved base had slightly higher pressures toward its edges but much lower pressures near its center, the result being no net improvement over the simply concaved base.

Afterbody Drag

Figure 17, a plot of afterbody pressure-drag coefficient as a function of Mach number, is included to help compare the drag characteristics of the different base and boattail combinations. Since recessing the base does not affect the boattail pressures, base concavity has the same effect on afterbody drag as it does on base drag; thus the trends for base and afterbody drag are the same.

As a matter of interest in determining the drag penalty incurred in truncating a cone, a plot of afterbody pressure-drag coefficient as a function of Mach number is presented in figure 18 for a fully conical afterbody with a boattail angle of 10° and for the two truncated afterbodies with boattail angles of 10° and open bases. The configurations with open bases were the minimum-drag configurations for the afterbodies with boattail angles of 10°, so the drag penalties shown in figure 18 would be the minimum incurred in this investigation for truncating a fully conical afterbody to values of L/D_m of 1.0 and 1.5. As with the base-drag plots, the drag for figures 17 and 18 was obtained by integrating the pressures of the top row of orifices only and no skin-friction drag was included.

Comparison of Pressure Drag With Balance Drag

The total afterbody drag coefficient computed from the balance measurement is presented as a function of Mach number in figure 19. As explained in the section "Data Reduction," the balance drag is the total afterbody drag and includes the effects of asymmetry of pressures with ϕ and of skin friction on the boattail. Thus, as a comparison with figure 17 shows, the balance drag is higher than the afterbody pressure drag, but the trends of the two agree very well.

In order to check the agreement of drag computed from the balance measurement and that computed from pressures, the computed total afterbody drag coefficient was obtained for an afterbody with $L/D_m = 1.5$, $\beta = 5^{\circ}$, and a concave base $\left(c/R_b = 0.25\right)$. The computed total afterbody drag coefficient was obtained for this configuration by using the integration of all the pressure-area terms for all the rows of orifices on its boattail and base, plus the skin-friction drag on its boattail, which was calculated on the basis of turbulent-boundary-layer theory. A comparison of this drag coefficient with that obtained from the balance is presented in figure 20, where the drags computed from the pressure and balance data are seen to agree very well.

Flow Model

A possible explanation of the fact that recessing the base reduces the base drag may be seen by considering figure 21(a), a sketch of the axisymmetric flow at a flat base in a viscous supersonic stream. As explained in reference 8, the flow outside of streamline AB passes downstream whereas the flow inside streamline AB is a relatively dead air region with a ring-vortex type of motion in the direction of the arrows. Viscous mixing takes place along AB, with the pressure in the eddy behind the base being determined by the scavenging action of the viscous mixing and the need of the flow to negotiate the pressure rise of the trailing shock.

References 2 and 9 indicate that for two-dimensional subsonic flow, the base cavity increases the base pressure by reducing the strength of the vortex street which forms behind bluff bodies at certain Reynolds numbers. Reference 9 also indicates that, according to this theory, in supersonic flow there is no mechanism for the base cavity to reduce drag, since the base eddy is trapped and no vortices are shed.

In axisymmetric subsonic flow, as opposed to two-dimensional subsonic flow, over bluff afterbodies, the base seems less likely to shed vortices in a stable configuration. This result seems to be borne out in reference 10 where the base-pressure variations with no jet flow were random in character at a free-stream Mach number of 0.5. Possibly, then, in axisymmetric flow the base cavity turns the circulatory flow at the edge of the base in a direction parallel to the flow off the boattail, as shown in figure 21(b). This action reduces the viscous mixing along streamline AB and causes AB to tend more toward the axis and hence be shorter. Thus it appears that there would be less scavenging of air from the base region and the base pressure would be increased.

CONCLUSIONS

An investigation was conducted in the Langley 16-foot transonic tunnel to determine the effects on base drag of recessing the base of an axisymmetric body. The conclusions reached from that investigation are as follows:

1. Over the range of Mach numbers from 0.3 to 1.3, and for boattail angles of 0° to 10°, recessing the base of an axisymmetric body with a truncated conical boattail causes an increase in base pressure and hence a decrease in base drag. The maximum increase in base pressure coefficient derived from recessing the base varied from 0.01 to 0.03 depending on the boattail.

2. In general, for a given boattail angle and length, base pressure increases with increasing base concavity up to a particular amount of concavity, but, beyond this amount, further concaving the base has little or no effect.

3. In the test range of boattail angles (0° to 10°), the steeper boattail angles generally require a greater ratio of base concavity to base radius to derive the maximum base-pressure benefits from recessing the base than do the shallower boattail angles.

4. For boattail angles of 0° to 10°, recessing the base has practically no effect on boattail pressures.

Langley Research Center,
National Aeronautics and Space Administration,
Langley Station, Hampton, Va., May 8, 1968,
720-03-00-01-23.

REFERENCES

1. Sedney, R.: Review of Base Drag. The Fluid Dynamic Aspects of Ballistics, AGARD Conf. Proc. No. 10, Sept. 1966, pp. 211-240.

2. Nash, J. F.: A Discussion of Two-Dimensional Turbulent Base Flows. R. & M. No. 3468, Brit. A.R.C., 1967.

3. Corson, Blake W., Jr.; and Mercer, Charles E.: Static Thrust of an Annular Nozzle With a Concave Central Base. NASA TN D-418, 1960.

4. Mercer, Charles E.; and Simonson, Albert J.: Effect of Geometric Parameters on the Static Performance of an Annular Nozzle With a Concave Central Base. NASA TN D-1006, 1962.

5. Corson, Blake W., Jr.; and Mercer, Charles E.: Transonic Thrust and Drag Characteristics of an Annular Nozzle Having a Semitoroidal Concave Plug. NASA TM X-958, 1964.

6. Capone, Francis J.; and Coates, Edward M., Jr.: Determination of Boundary-Reflected-Disturbance Lengths in the Langley 16-Foot Transonic Tunnel. NASA TN D-4153, 1967.

7. Goodyer, M. J.: Some Experimental Investigations Into the Drag Effects of Modifications to the Blunt Base of a Body of Revolution. ISAV Rep. No. 150, Univ. of Southampton, July 1966.

8. Chapman, Dean R.: An Analysis of Base Pressure at Supersonic Velocities and Comparison With Experiment. NACA Rep. 1051, 1951. (Supersedes NACA TN 2137.)

9. Nash, J. F.; Quincey, V. G.; and Callinan, J.: Experiments on Two-Dimensional Base Flow at Subsonic and Transonic Speeds. NPL Rep. 1070, Brit. A.R.C., Jan. 21, 1963.

10. Rossiter, J. E.; and Kurn, A. G.: Wind Tunnel Measurements of the Effect of a Jet on the Time Average and Unsteady Pressures on the Base of a Bluff Afterbody. C.P. No. 903, Brit. A.R.C., 1967.

TABLE 1.- BOATTAIL-SURFACE ORIFICE LOCATIONS

Boattail with $L/D_m = 1.0$	
ϕ, deg	x/D_m for $\beta = 3^\circ$, 5°, and 10°
0 and 90	-0.02
	.02
	.08
	.25
	.50
	.75
	.97
45, 135, 157.5, and 180	.02
	.25
	.50
	.75
	.97

Boattail with $L/D_m = 1.5$			
ϕ, deg	x/D_m for -		
	$\beta = 0^\circ$	$\beta = 3^\circ$ and 5°	$\beta = 10^\circ$
0 and 180	0.13	-0.07	-0.07
	.30	.02	.02
	.47	.12	.12
	.63	.37	.36
	.80	.60	.59
	.97	.75	.74
	1.13	1.00	.98
	1.30	1.25	1.23
	1.47	1.45	1.43
22.5		.02	.02
		.12	.12
		.37	.36
		.60	.59
		.75	.74
		1.00	.98
		1.25	1.23
		1.31	1.30
45	.13	.02	.02
	.30	.12	.12
	.47	.37	.36
	.63	.60	.59
	.80	.75	.74
	.97	1.00	.98
	1.13	1.25	1.23
		1.31	1.30
90	.13	.02	.02
	.30	.12	.12
	.47	.37	.36
	.63	.60	.59
	.80	.75	.74
	.97	1.00	.98
	1.13	1.25	1.23
	1.30	1.45	1.43
	1.47		
135	.13		
	.30		
	.47		
	.63		
	.80		
	.97		
	1.13		

Full cone	
ϕ, deg	x/D_m for $\beta = 10^\circ$
0 and 180	-0.07
	.02
	.12
	.25
	.41
	.73
	1.07
	1.40
	1.72
	2.22
	2.71
45 and 135	.02
	.12
	.25
	.41
	.74
	1.07
	1.40
	1.72
	2.22
90	.02
	.12
	.25
	.41
	.74
	1.07
	1.40
	1.72
	2.22
	2.71

TABLE 2.- BASE ORIFICE LOCATIONS[a]

ϕ, deg	r/R_b for configuration –																		
	4	5	7	8	9	10	12	13	15	16	17	19	20	22	23	24	25	27	28
0, 90, and 180	0	0	0	0	0	0	0	0	0	0	0	0	0	0	0	0	0	0	0
↓	.45	.23	.48	.08	.24	.24	.46	.23	.50	.25	.25	.48	.24	.45	.09	.23	.23	.50	.25
↓	.91	.46	.95	.24	.48	.48	.89	.46	.92	.50	.50	.88	.48	.90	.23	.45	.45	.90	.50
↓		.69		.50	.73	.73		.69		.66	.75		.72		.50	.66	.68		.75
↓		.89		.75	.89	.87		.89		.80	.87		.88		.76	.88	.88		.89
↓		.93		.91		.93		.94		.92	.93		.93		.90		.92		
45									.50	.50	.50	.48	.48	.45	.23	.23	.45	.50	.25
↓									.92	.80	.87	.88	.88	.90	.76	.45	.88	.90	.50
↓										.92	.93					.66			.75
↓																.88			.89
135	.45		.48				.46												
↓	.91		.95				.89												

[a] The exact location of the base orifices of the open-base configurations (6, 11, 14, 18, 21, 26, and 29) was relatively unimportant and they were not purposely placed in any special radial position.

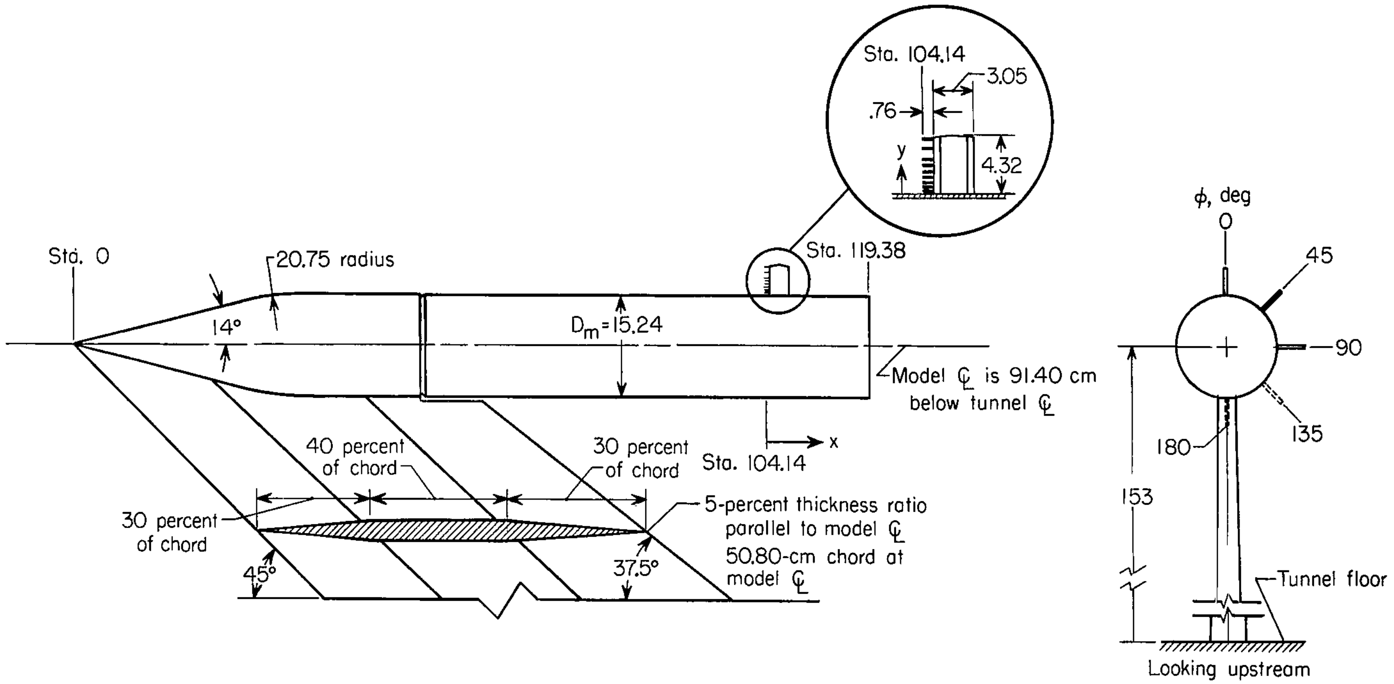

Configuration	Description
1	Cylindrical survey body
2	Cylindrical survey body with boundary-layer rakes at 0°, 45°, and 90°
3	Cylindrical survey body with boundary-layer rakes at 90°, 135°, and 180°

Cylinder orifice locations			
Configuration 1		Configurations 2 and 3	
φ, deg	x/D_m	φ, deg	x/D_m
0, 90, and 180	−0.37 −0.20 −0.03 .13 .30 .47 .63 .80 .97	0, 90, 135 and 180	−0.75 −0.50 −0.25 0
45 and 135	−0.37 −0.20 −0.03 .13 .30 .47 .63	157.5	−0.75 −0.25

Boundary-layer rake tubes	
y	y/D_m
0.25	0.017
.51	.033
.76	.050
1.14	.075
1.52	.100
2.03	.133
2.54	.167
3.30	.217
4.06	.267

Figure 1.- Sketch of model showing details of boundary-layer and flow-field survey configurations. (All dimensions are in centimeters unless otherwise noted.)

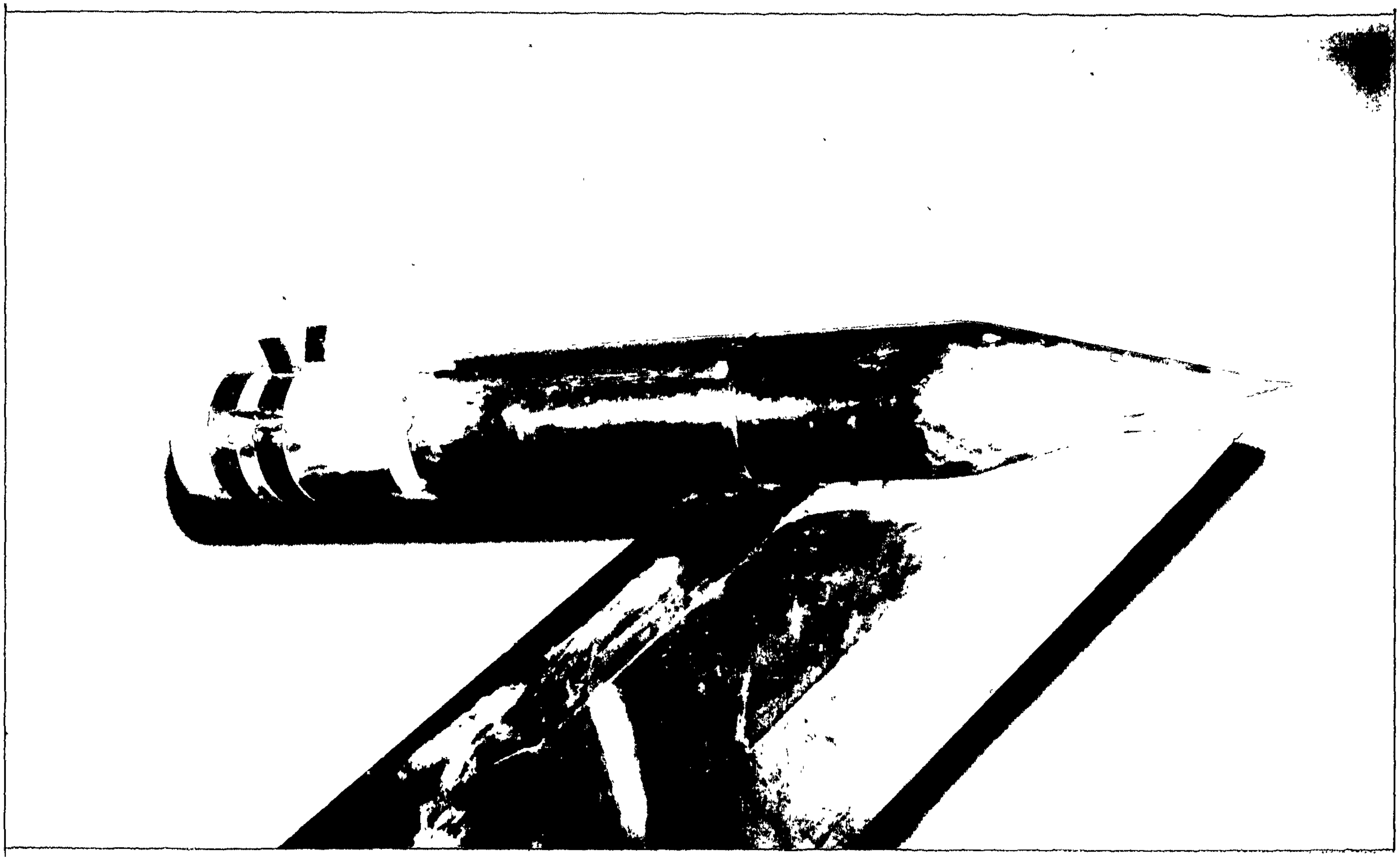

Figure 2.- Photograph of model with configuration 2 (cylindrical afterbody with boundary-layer rakes at 0°, 45°, and 90°) installed. L-67-1985

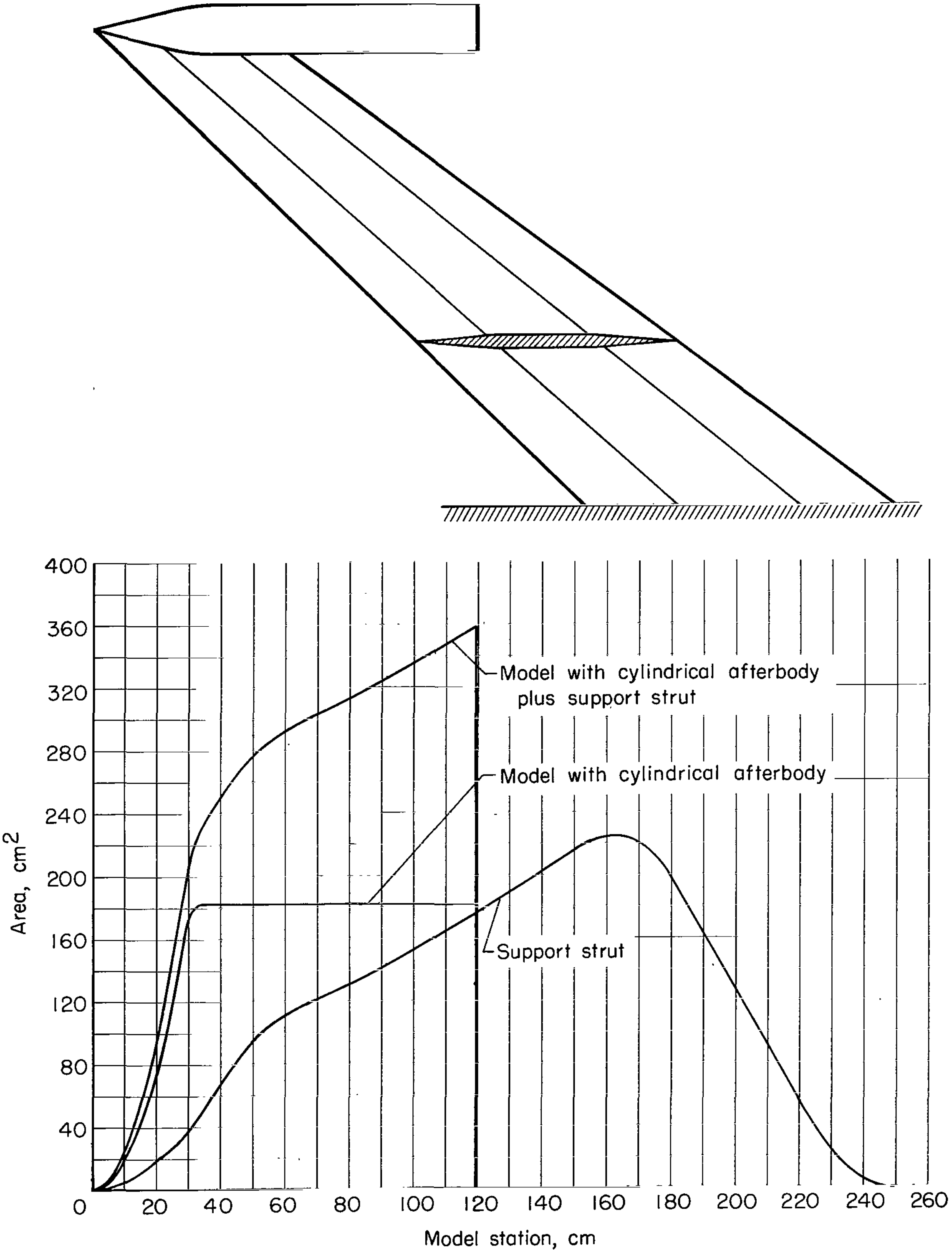

Figure 3.- Area distributions of support strut and model with cylindrical afterbody.

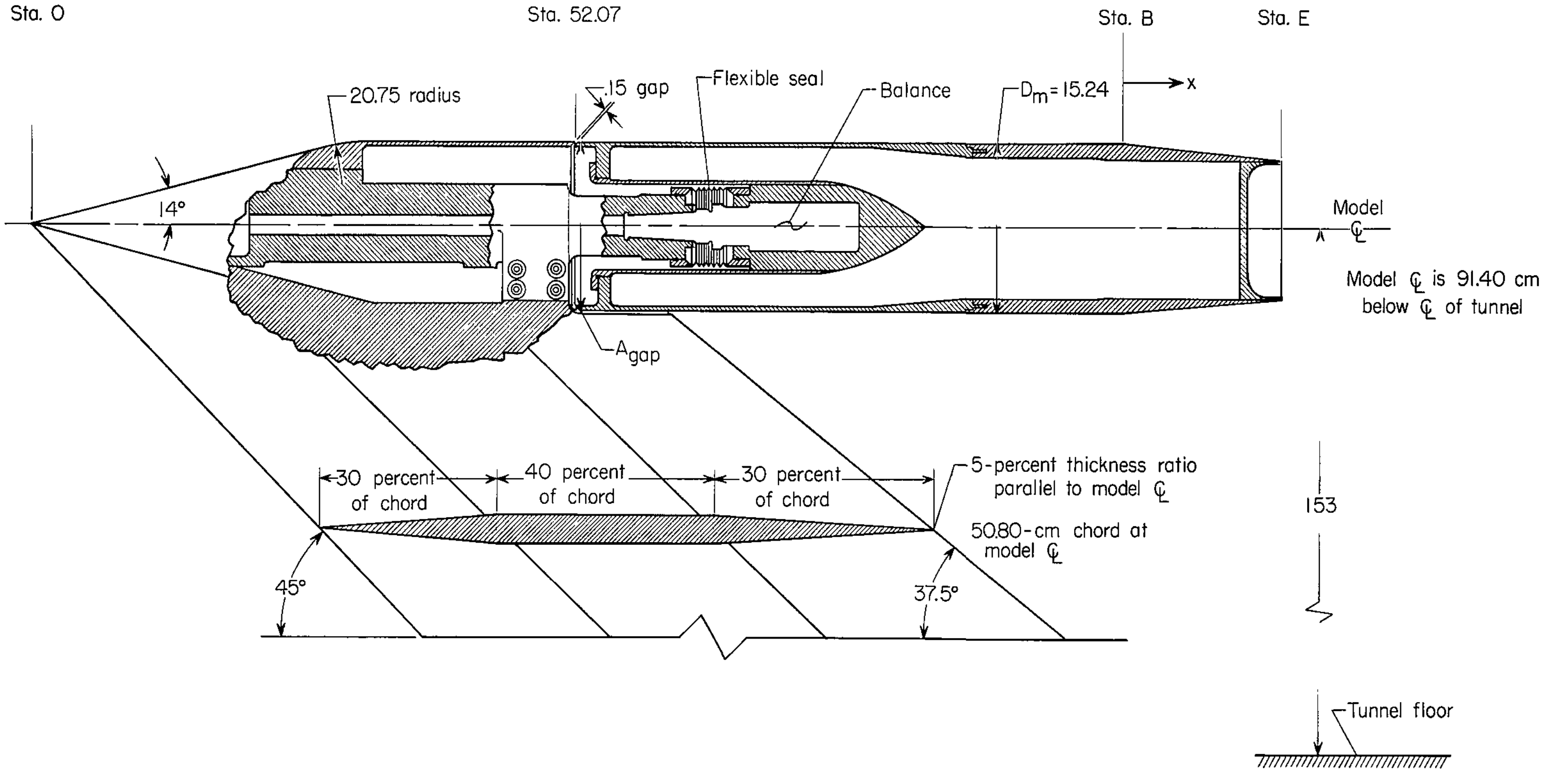

Figure 4.- Sketch showing geometry of model pertinent to investigation of the effects of recessing the base. (All dimensions are in centimeters unless otherwise noted.)

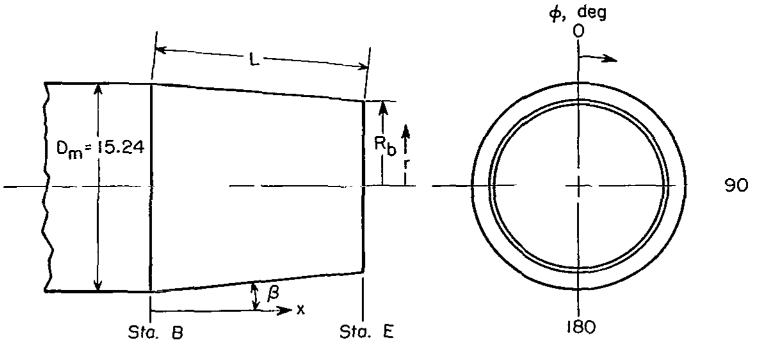

Afterbody geometry

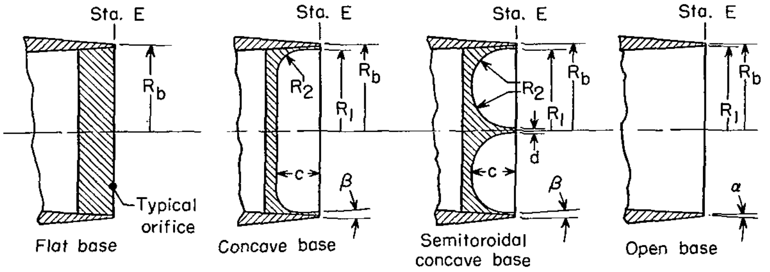

Base geometry

Note: Geometry of cone with boattail angle of 10 degrees not shown.

Configuration	Type base	Dimension										
		L/D_m	Sta. B	β, deg	Sta. E	A_b/A_m	R_b	c/R_b	R_1	R_2	d	α, deg
4	Flat	1.0	104.14	3	119.38	0.80	6.82	0	—	—	—	—
5	Concave	1.0	104.14	3	119.38	0.80	6.82	0.25	6.47	0.44	—	—
6	Open	1.0	104.14	3	119.38	0.80	6.82	Open base	6.71	—	—	4.84
7	Flat	1.0	104.14	5	119.30	0.68	6.29	0	—	—	—	—
8	Semitoroidal concave	1.0	104.14	5	119.30	0.68	6.29	0.50	6.03	2.64	0.30	—
9	Concave	1.0	104.14	5	119.30	0.68	6.29	0.50	5.92	1.87	—	—
10	Concave	1.0	104.14	5	119.30	0.68	6.29	0.25	5.95	0.56	—	—
11	Open	1.0	104.14	5	119.30	0.68	6.29	Open base	6.18	—	—	3.23
12	Flat	1.0	104.14	10	119.15	0.43	4.97	0	—	—	—	—
13	Concave	1.0	104.14	10	119.15	0.43	4.97	0.25	4.61	0.36	—	—
14	Open	1.0	104.14	10	119.15	0.43	4.97	Open base	4.86	—	—	0.76
15	Flat	1.5	96.52	0	119.38	1.00	7.62	0	—	—	—	—
16	Concave	1.5	96.52	0	119.38	1.00	7.62	0.50	7.29	2.29	—	—
17	Concave	1.5	96.52	0	119.38	1.00	7.62	0.25	7.29	0.64	—	—
18	Open	1.5	96.52	0	119.38	1.00	7.62	Open base	7.37	—	—	0
19	Flat	1.5	96.52	3	119.35	0.70	6.38	0	—	—	—	—
20	Concave	1.5	96.52	3	119.35	0.70	6.38	0.25	6.14	0.59	—	—
21	Open	1.5	96.52	3	119.35	0.70	6.38	Open base	6.27	—	—	0
22	Flat	1.5	96.52	5	119.29	0.55	5.63	0	—	—	—	—
23	Semitoroidal concave	1.5	96.52	5	119.29	0.55	5.63	0.50	5.35	2.29	0.30	—
24	Concave	1.5	96.52	5	119.29	0.55	5.63	0.50	5.30	1.66	—	—
25	Concave	1.5	96.52	5	119.29	0.55	5.63	0.25	5.31	0.47	—	—
26	Open	1.5	96.52	5	119.29	0.55	5.63	Open base	5.48	—	—	0
27	Flat	1.5	96.52	10	119.03	0.23	3.65	0	—	—	—	—
28	Concave	1.5	96.52	10	119.03	0.23	3.65	0.25	3.30	0.28	—	—
29	Open	1.5	96.52	10	119.03	0.23	3.65	Open base	3.49	—	—	0
30	Cone	2.89	96.52	10	136.90	—	—	—	—	—	—	—

Figure 5.- Geometry and dimensions of afterbody configurations. (All dimensions are in centimeters unless otherwise noted.)

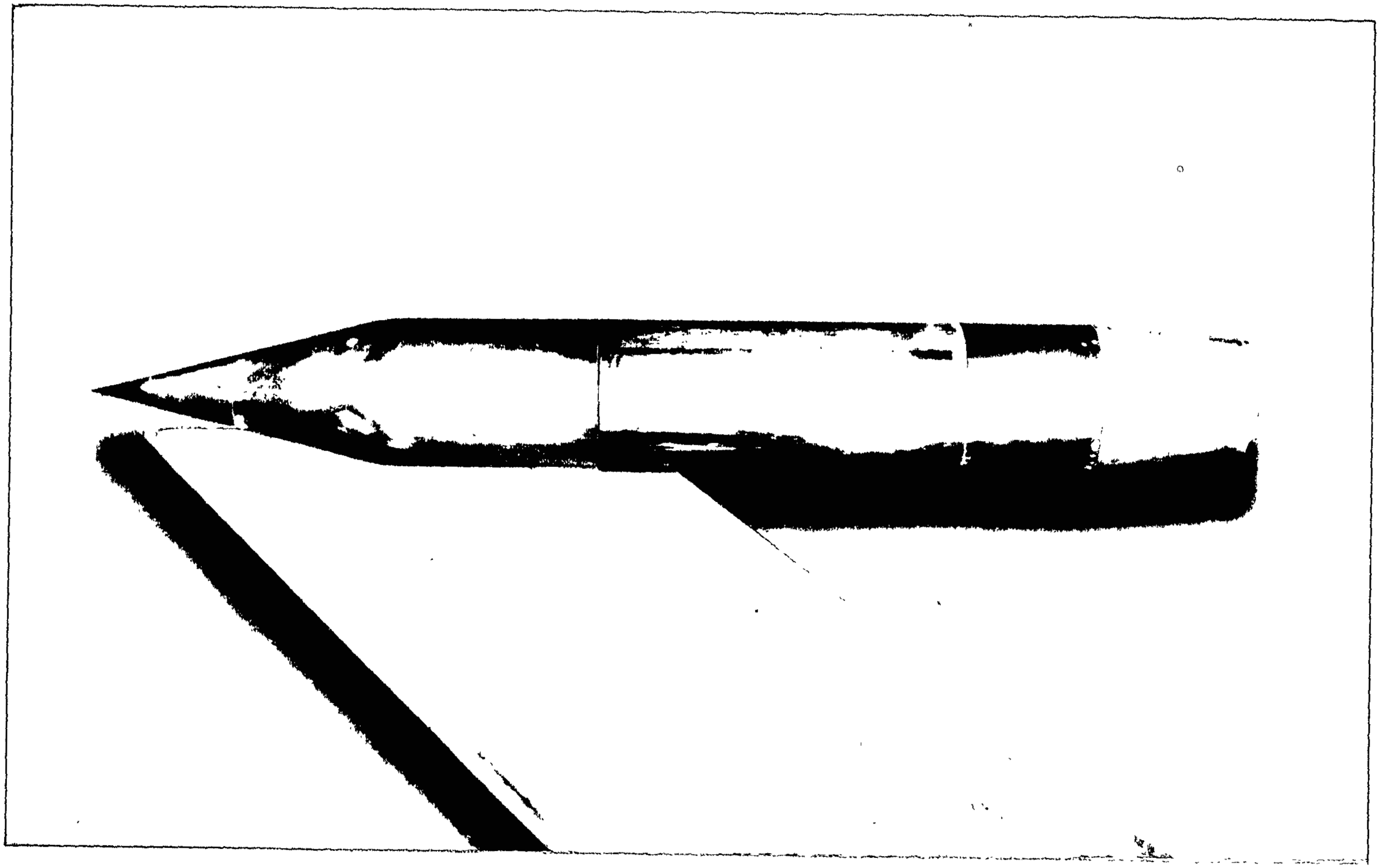

Figure 6.- Photograph of model having afterbody with $L/D_m = 1.0$ and $\beta = 5^{\circ}$.

L-67-1987

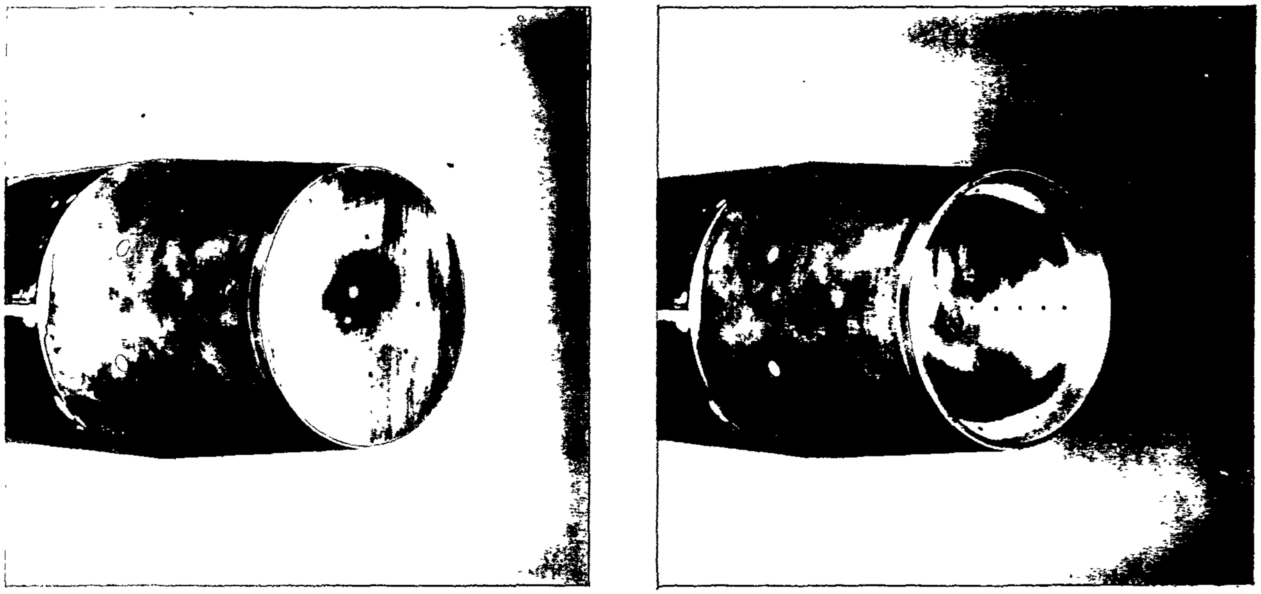

Flat base

Concave base

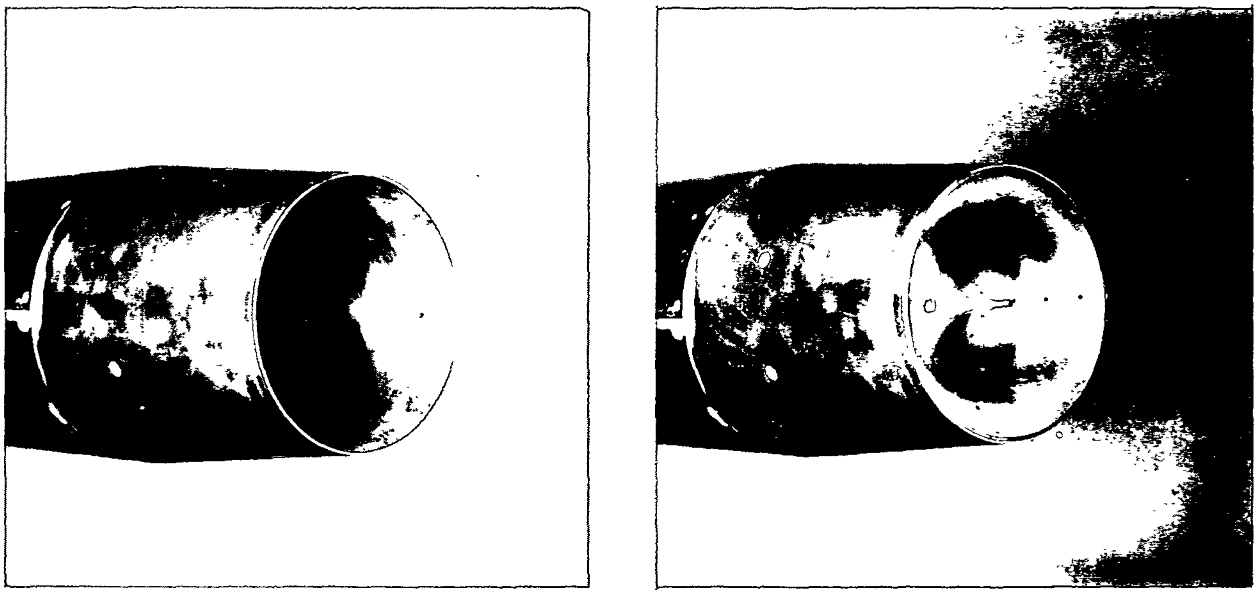

Open base

Semitoroidal
concave base

Figure 7.- Photographs of typical bases.

L-68-5636

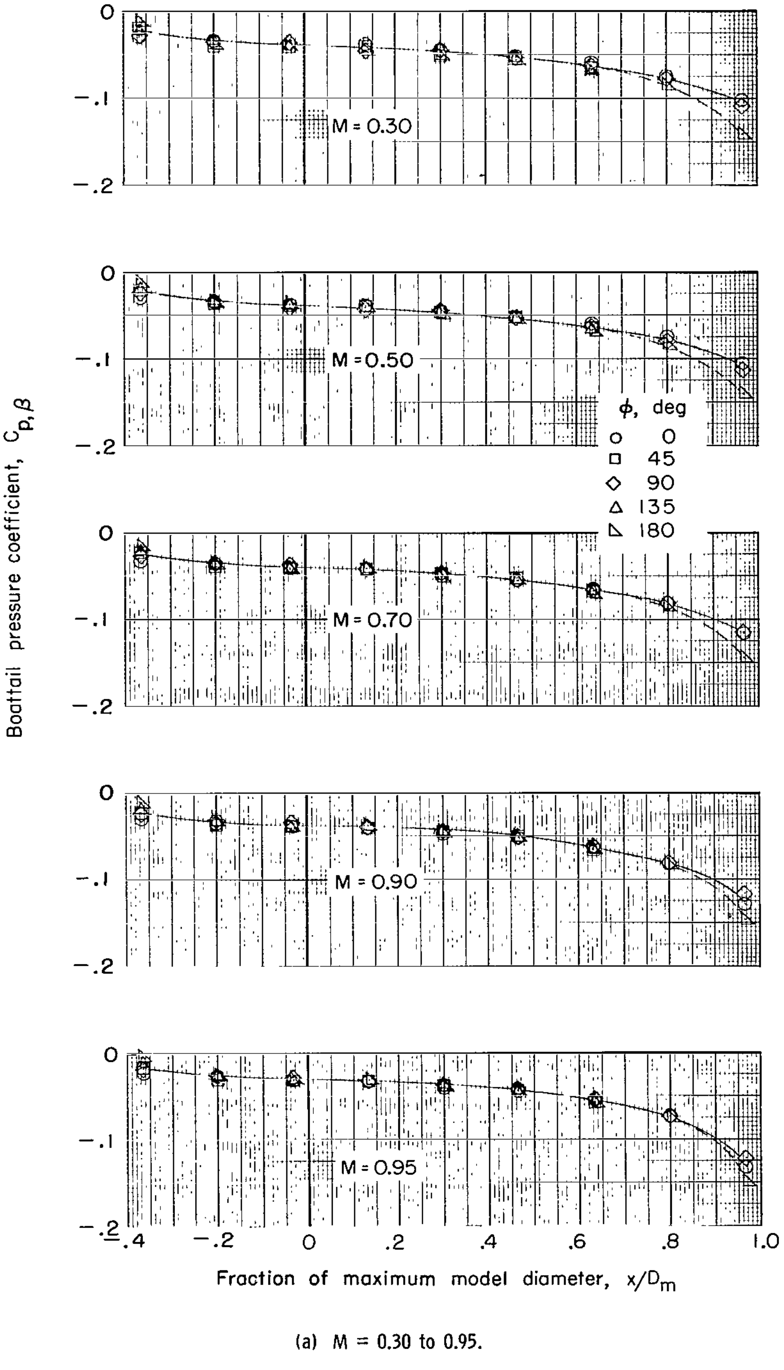

(a) M = 0.30 to 0.95.

Figure 8.- Typical boattail-pressure-coefficient distributions on a cylindrical afterbody with a flat base for various Mach numbers and values of Φ.

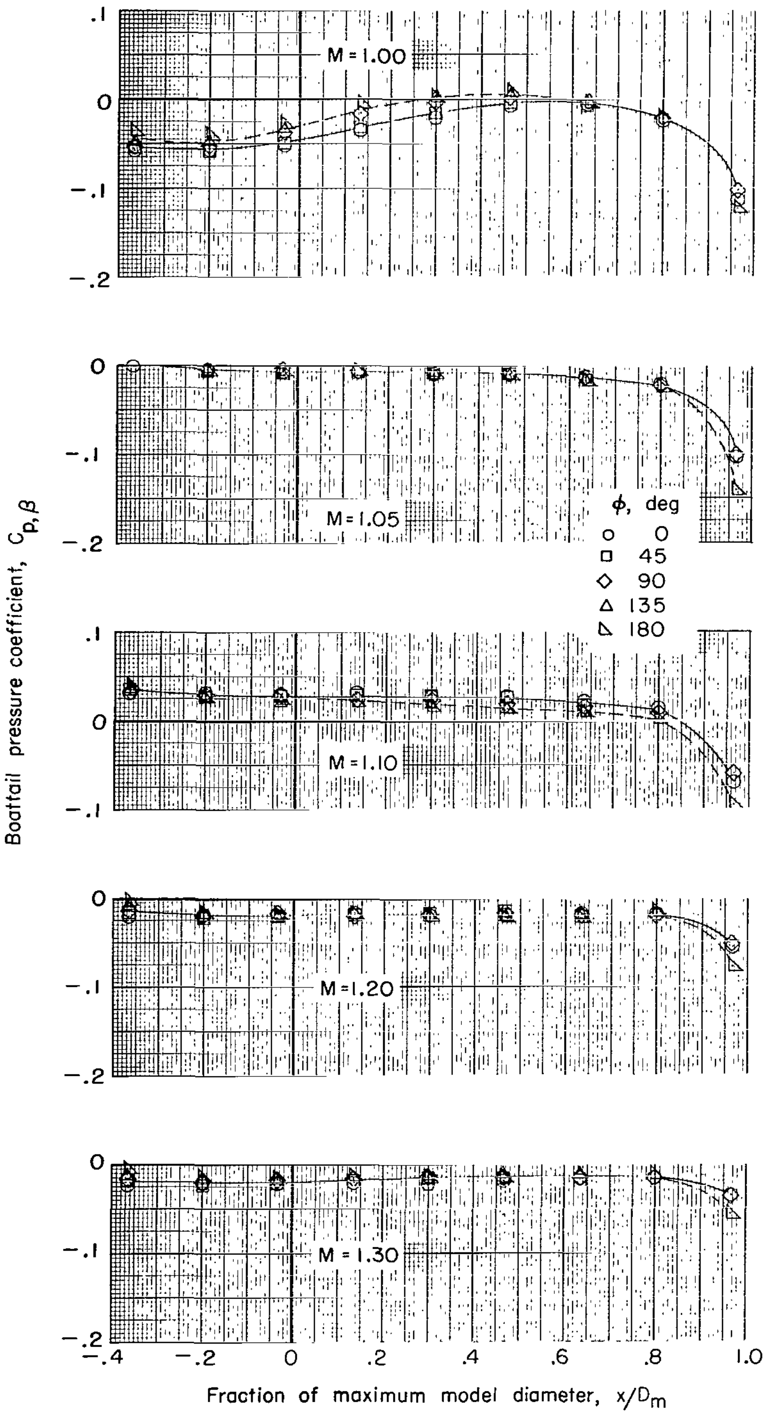

(b) M = 1.00 to 1.30.

Figure 8.- Concluded.

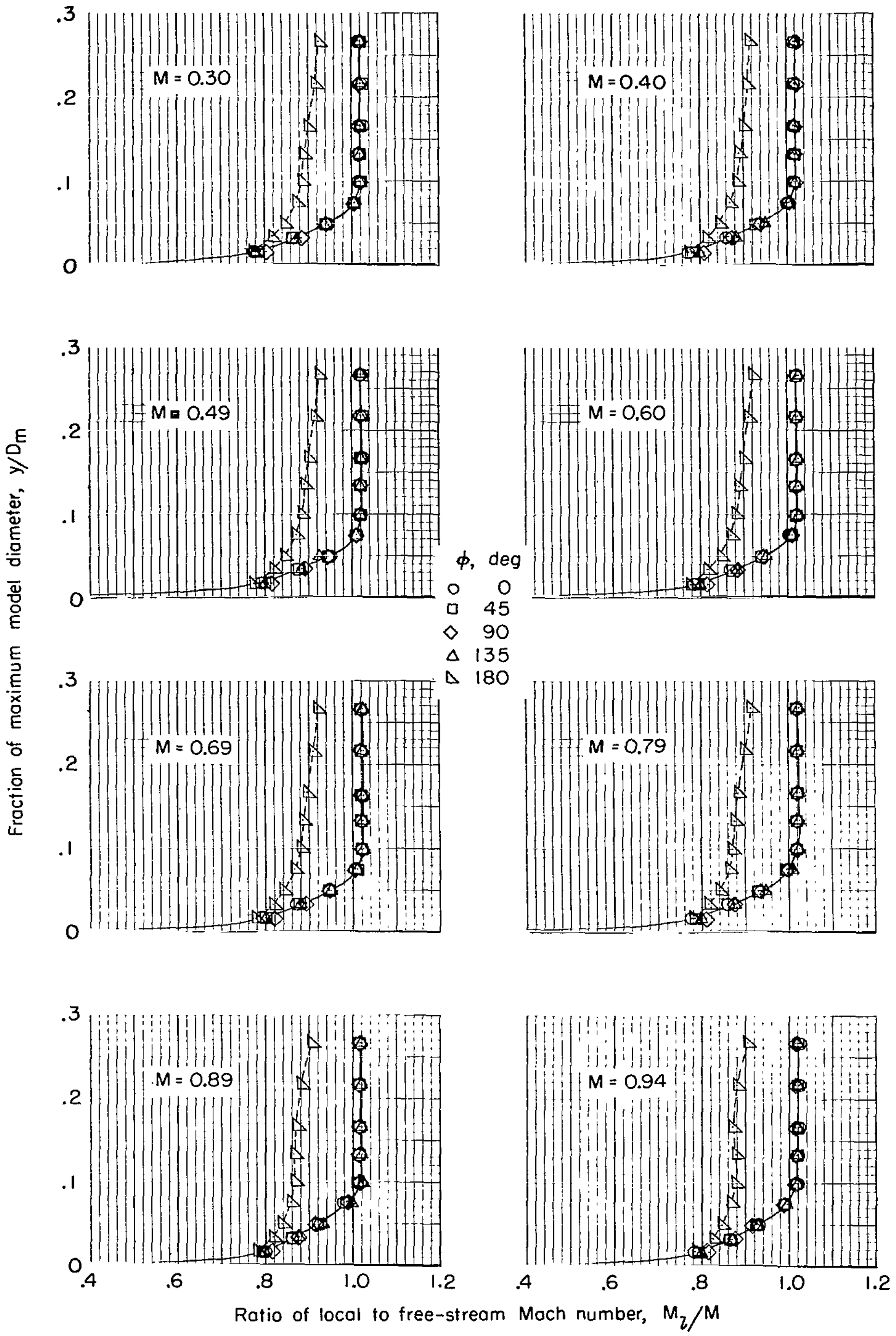

(a) M = 0.30 to 0.94.

Figure 9.- Typical boundary-layer Mach number profiles for a cylindrical afterbody at various free-stream Mach numbers. (Boundary-layer rakes are at model station 104.14.)

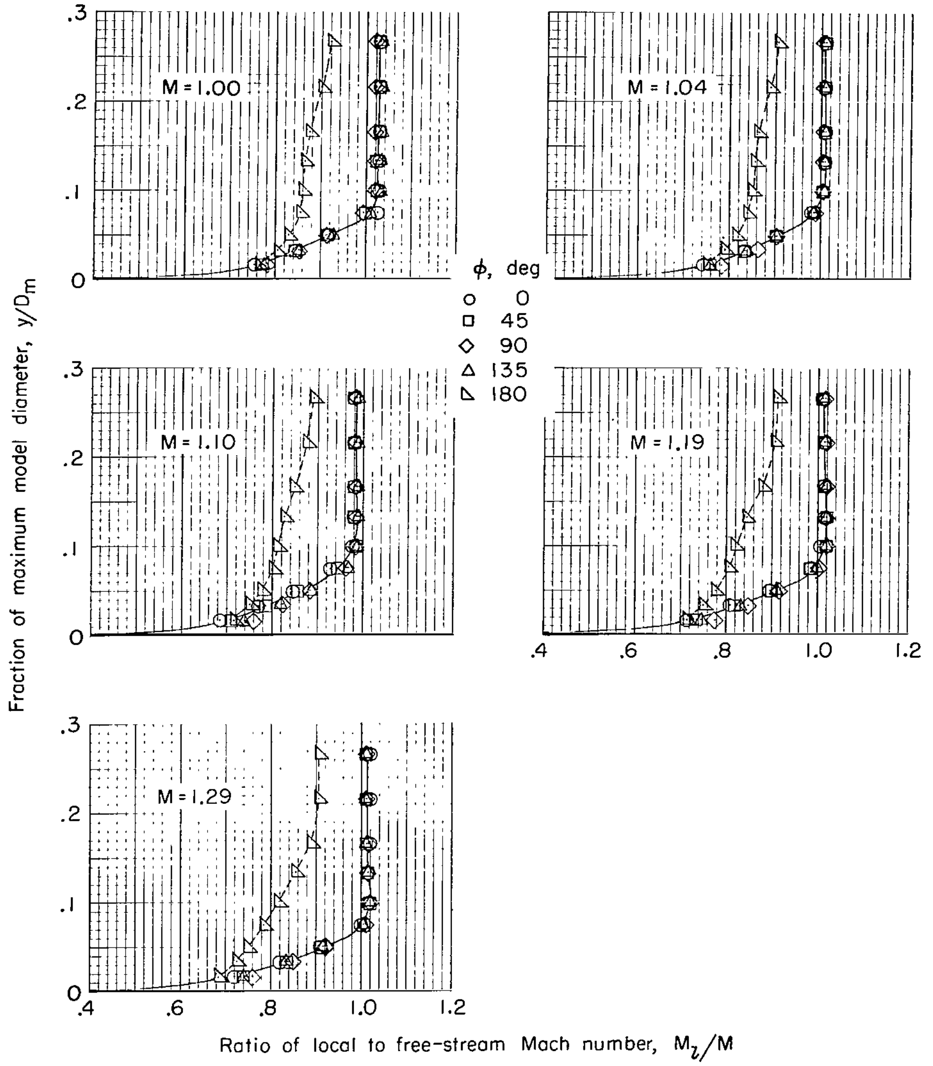

(b) M = 1.00 to 1.29.

Figure 9.- Concluded.

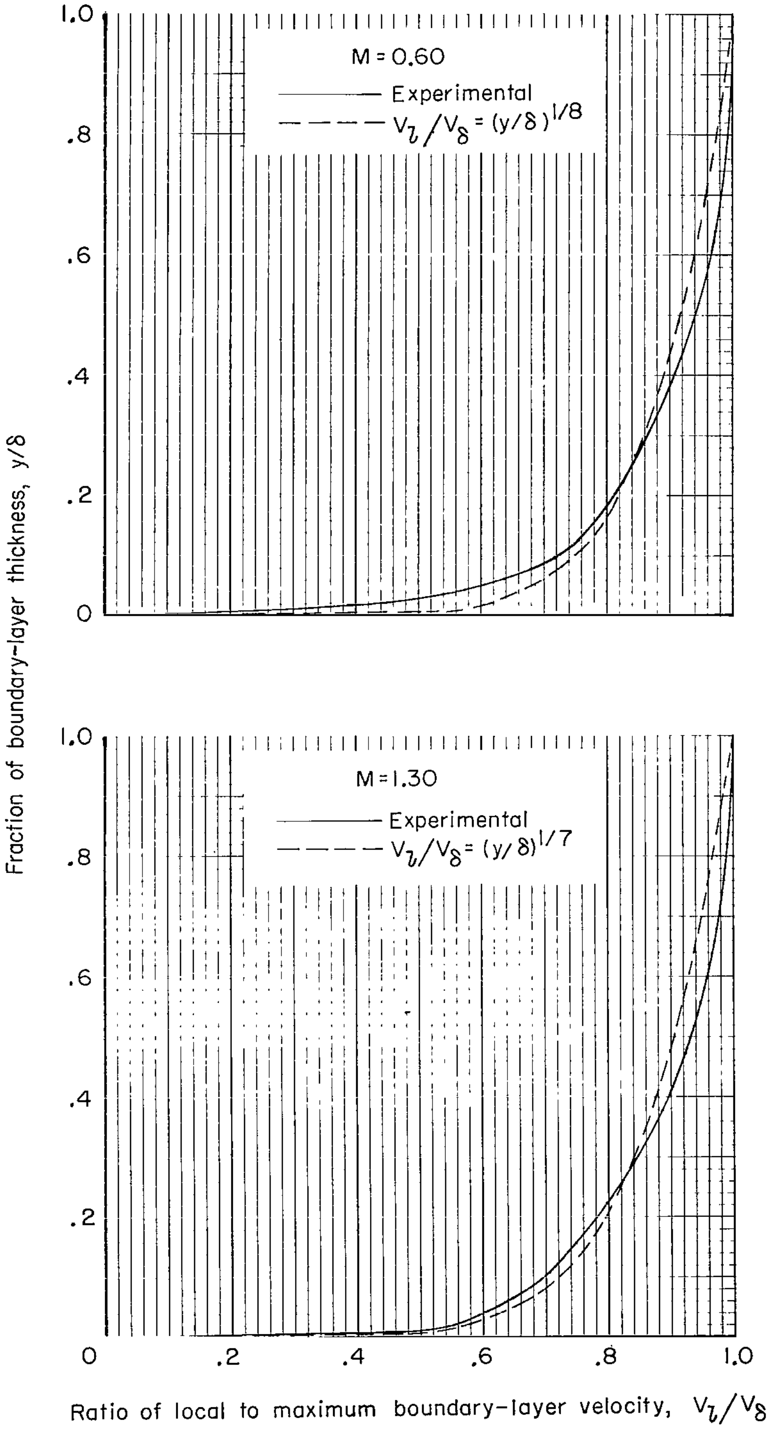

Figure 10.- Comparison of experimental and power-law-calculated boundary-layer profiles.

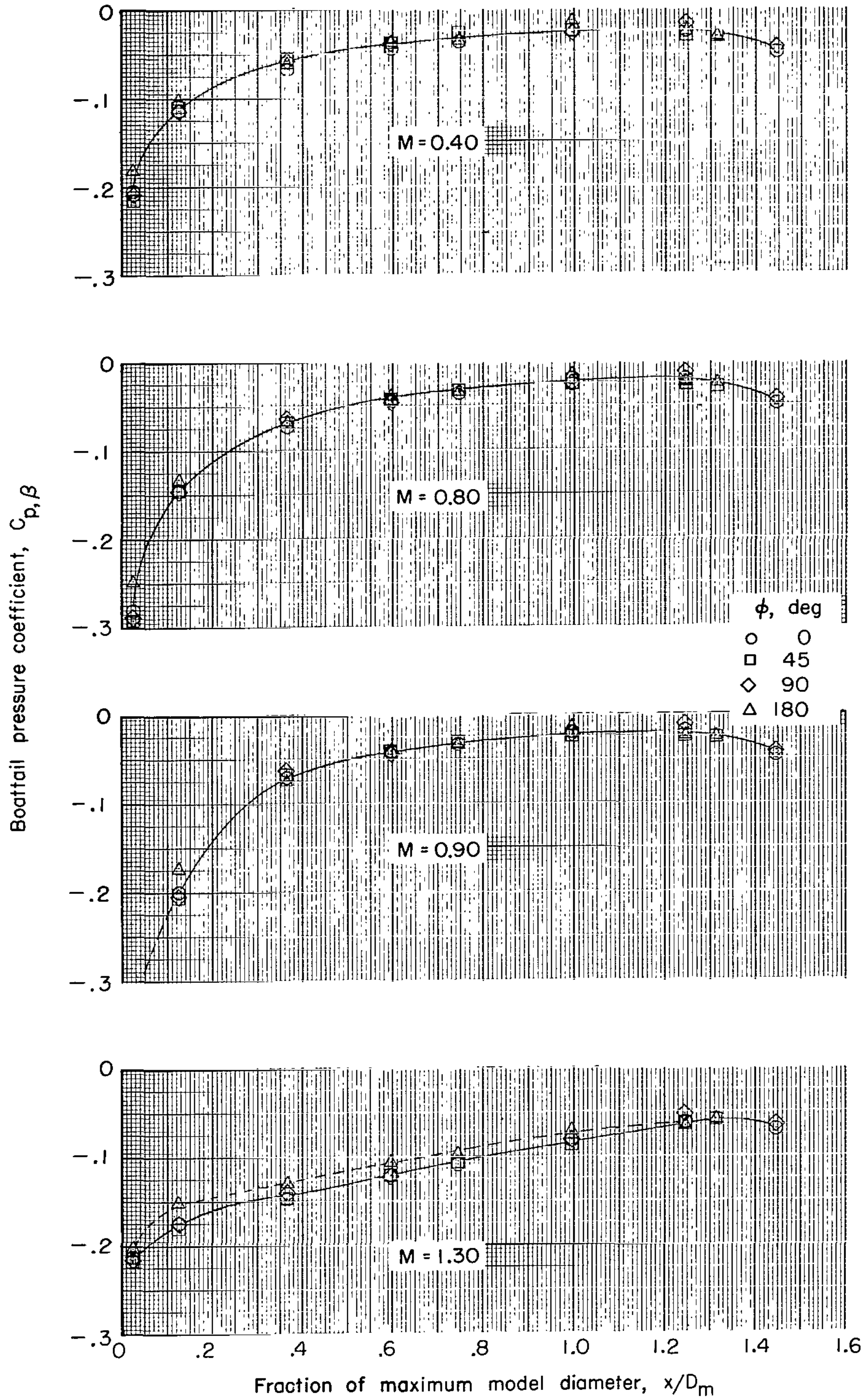

Figure 11.- Typical boattail-pressure-coefficient distributions for several Mach numbers and values of Φ. $L/D_m = 1.5$; $\beta = 5^0$; concave base $(c/R_b = 0.25)$.

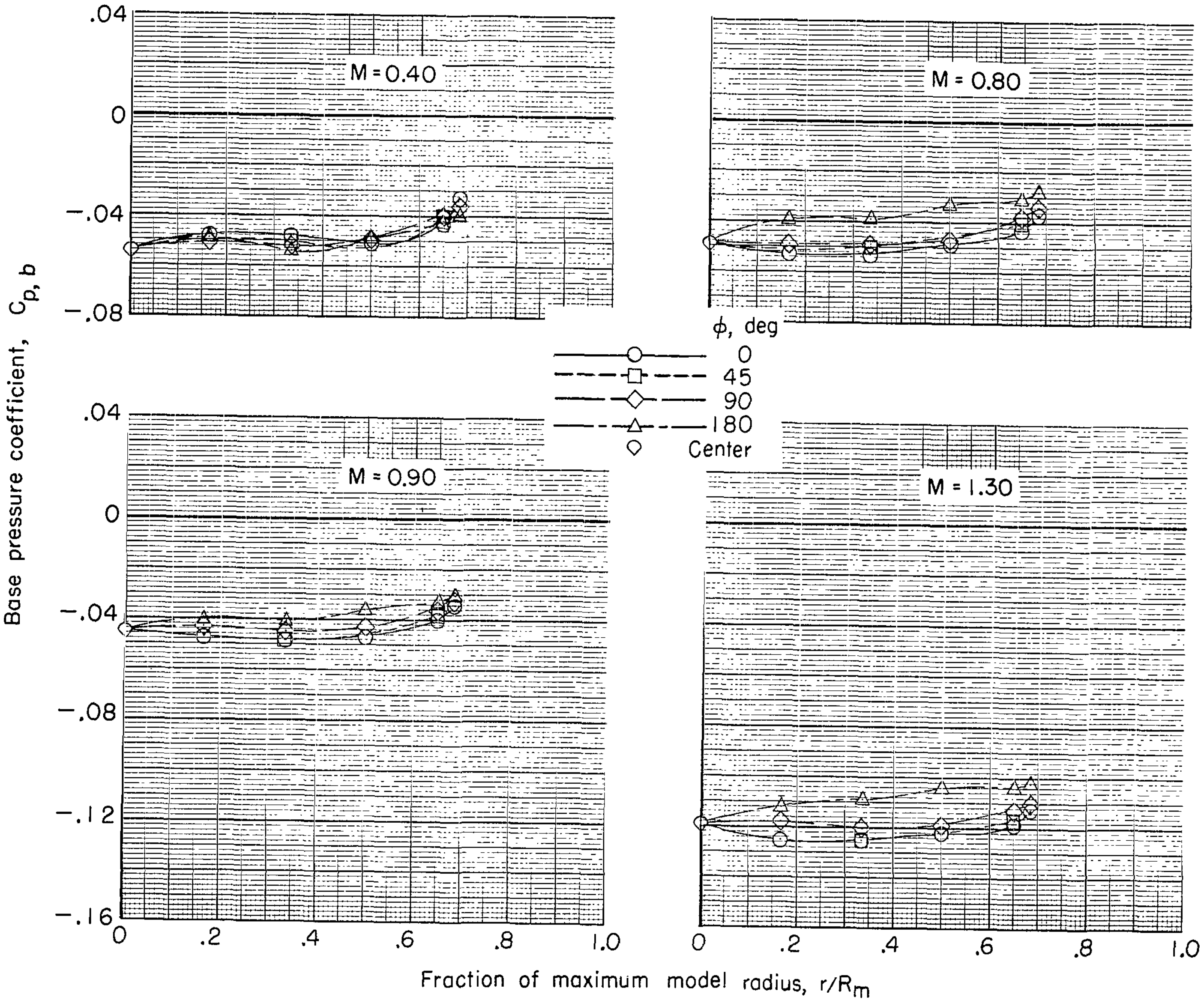

Figure 12.- Typical base-pressure-coefficient distributions for various Mach numbers and values of Φ. $L/D_m = 1.5$; $\beta = 5^0$; concave base $(c/R_b = 0.25)$.

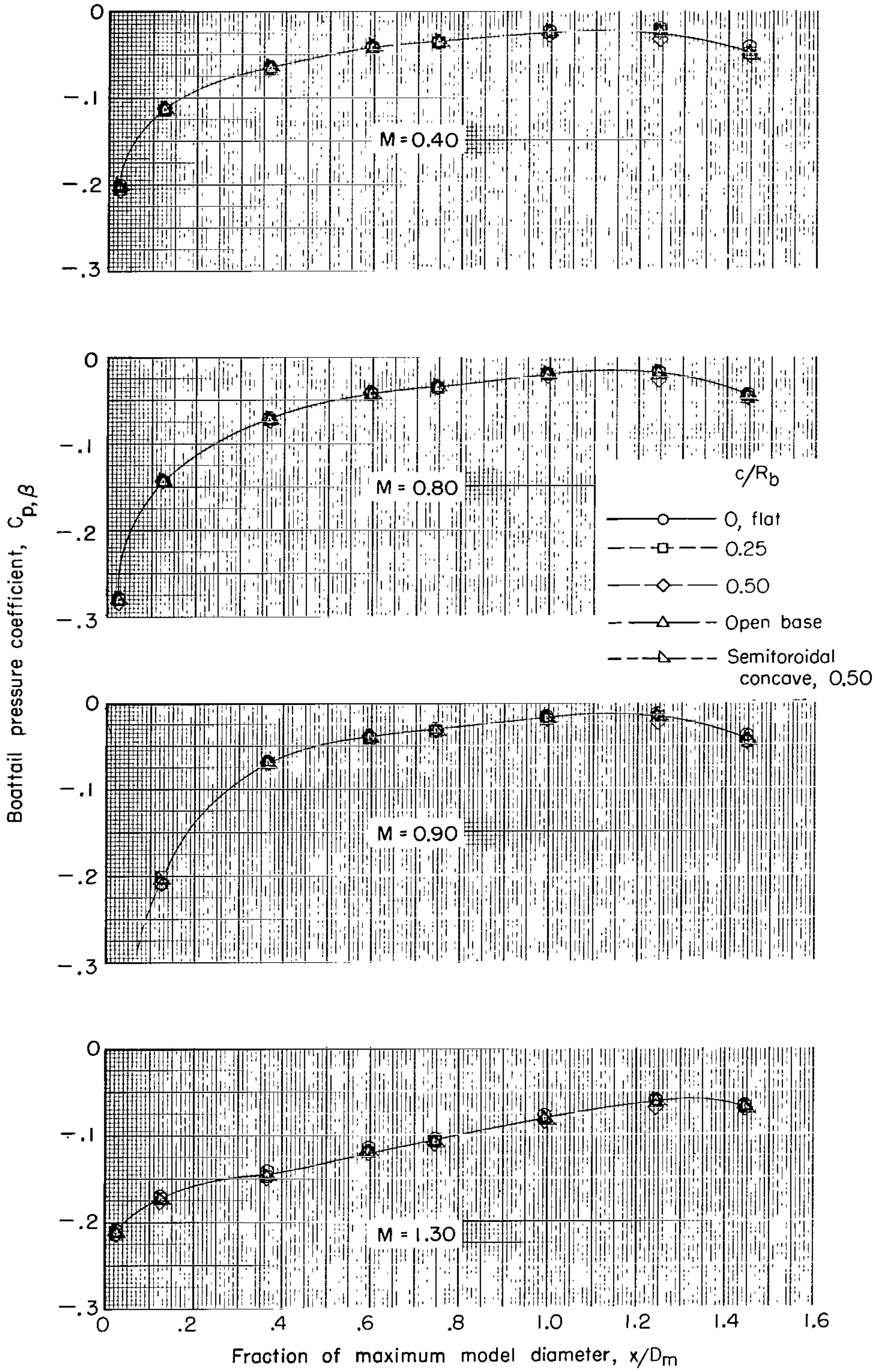

Figure 13.- Typical boattail-pressure-coefficient distributions for various base concavities and Mach numbers. $L/D_m = 1.5$; $\beta = 5^0$; orifice rows at $\Phi = 0^0$.

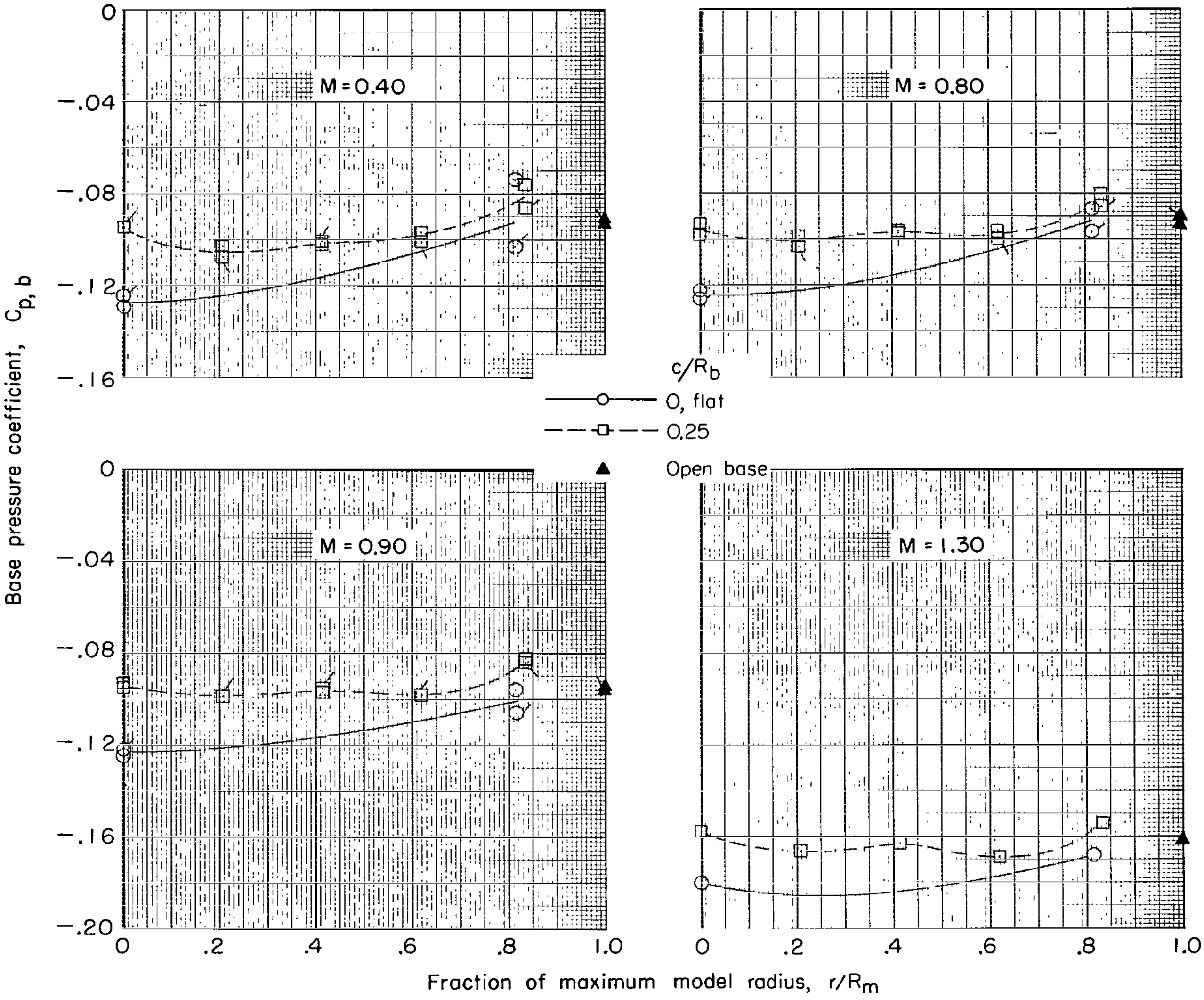

(a) $L/D_m = 1.0$; $\beta = 5^0$; $A_b/A_m = 0.68$.

Figure 14.- Base-pressure-coefficient distributions for various configurations and Mach numbers, with orifice rows at $\Phi = 0^0$. (Flagged symbols indicate data taken as Mach number was decreased.)

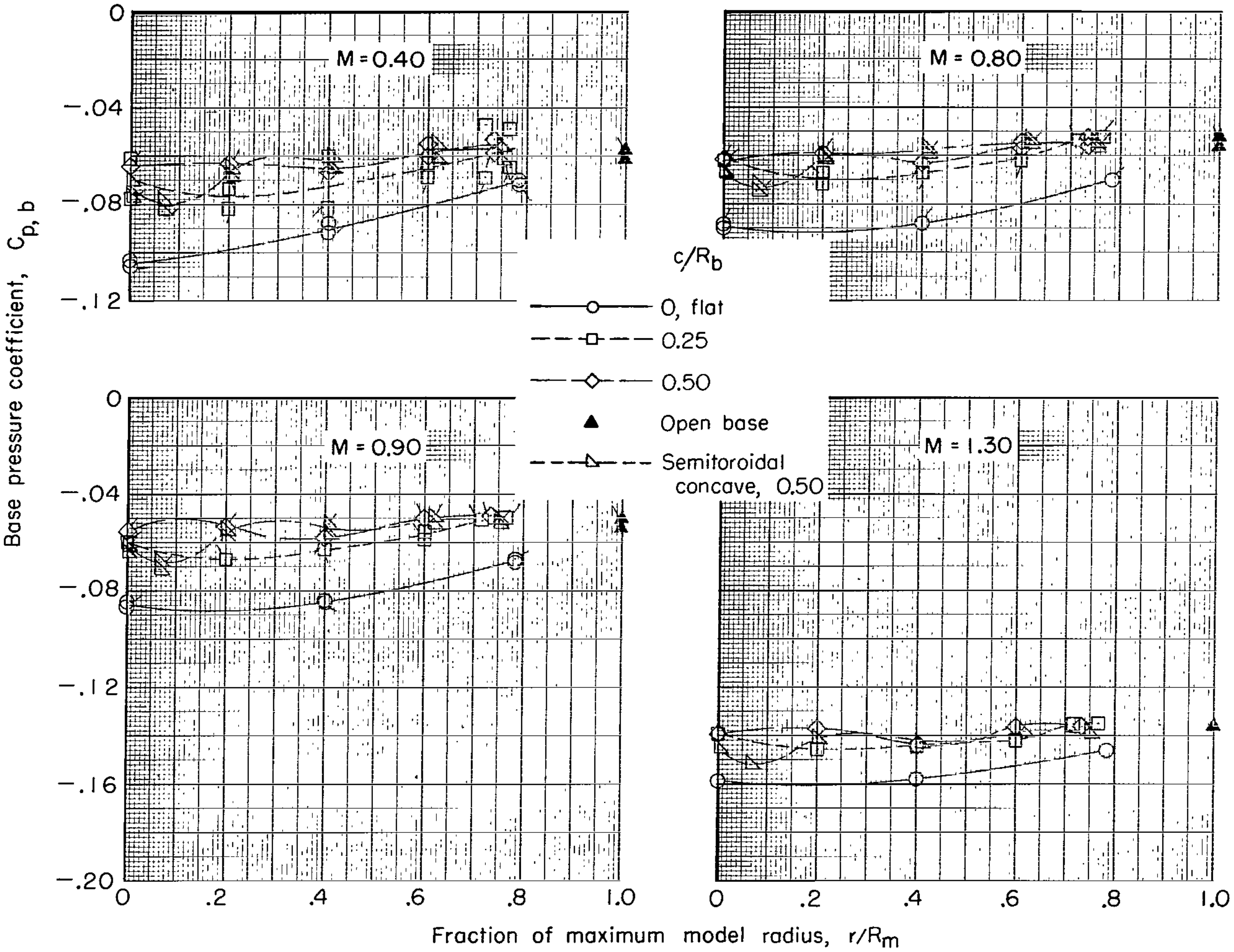

(b) $L/D_m = 1.0$; $\beta = 5^0$; $A_b/A_m = 0.68$.

Figure 14.- Continued.

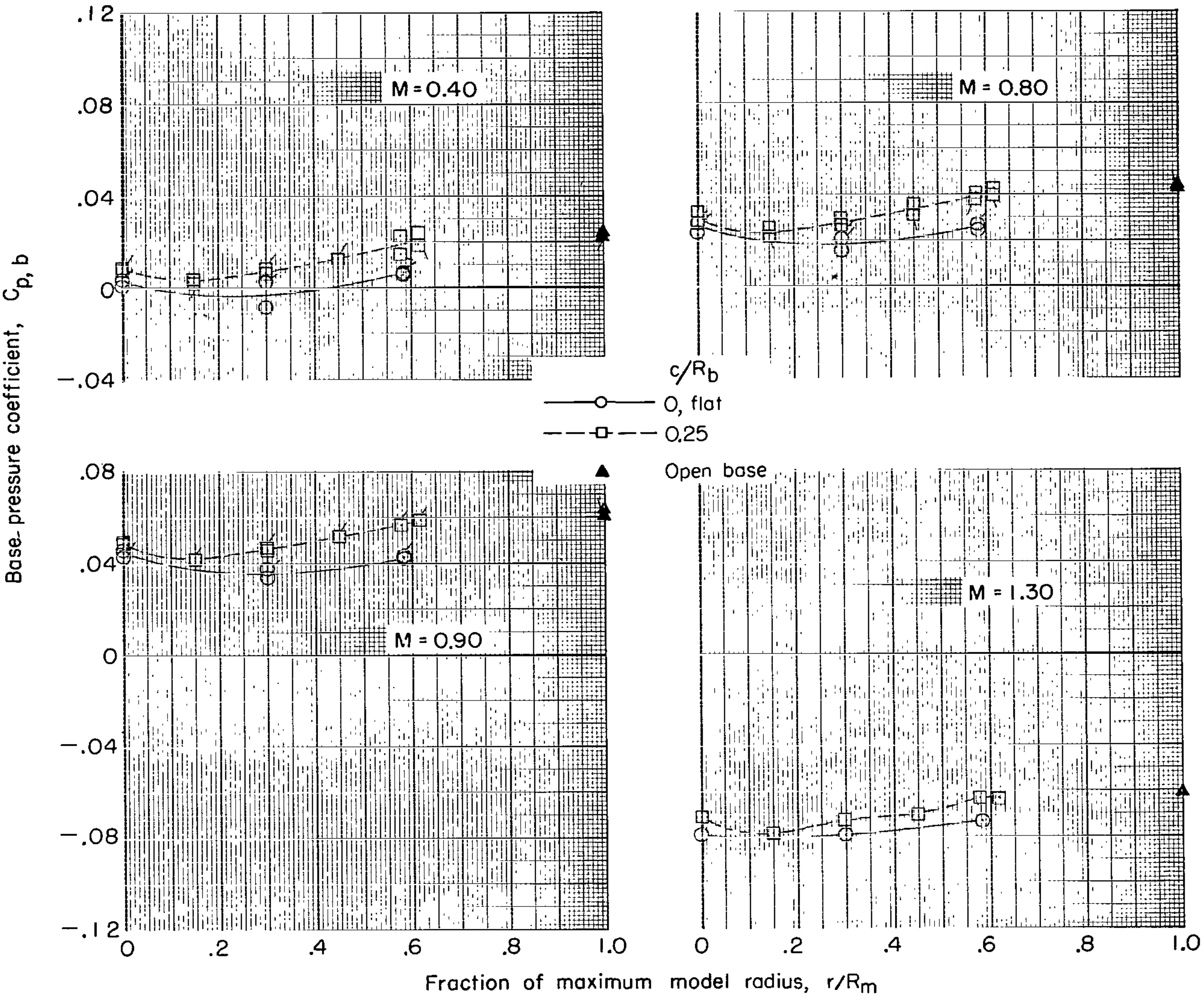

(c) $L/D_m = 1.0$; $\beta = 10^0$; $A_b/A_m = 0.43$.

Figure 14.- Continued.

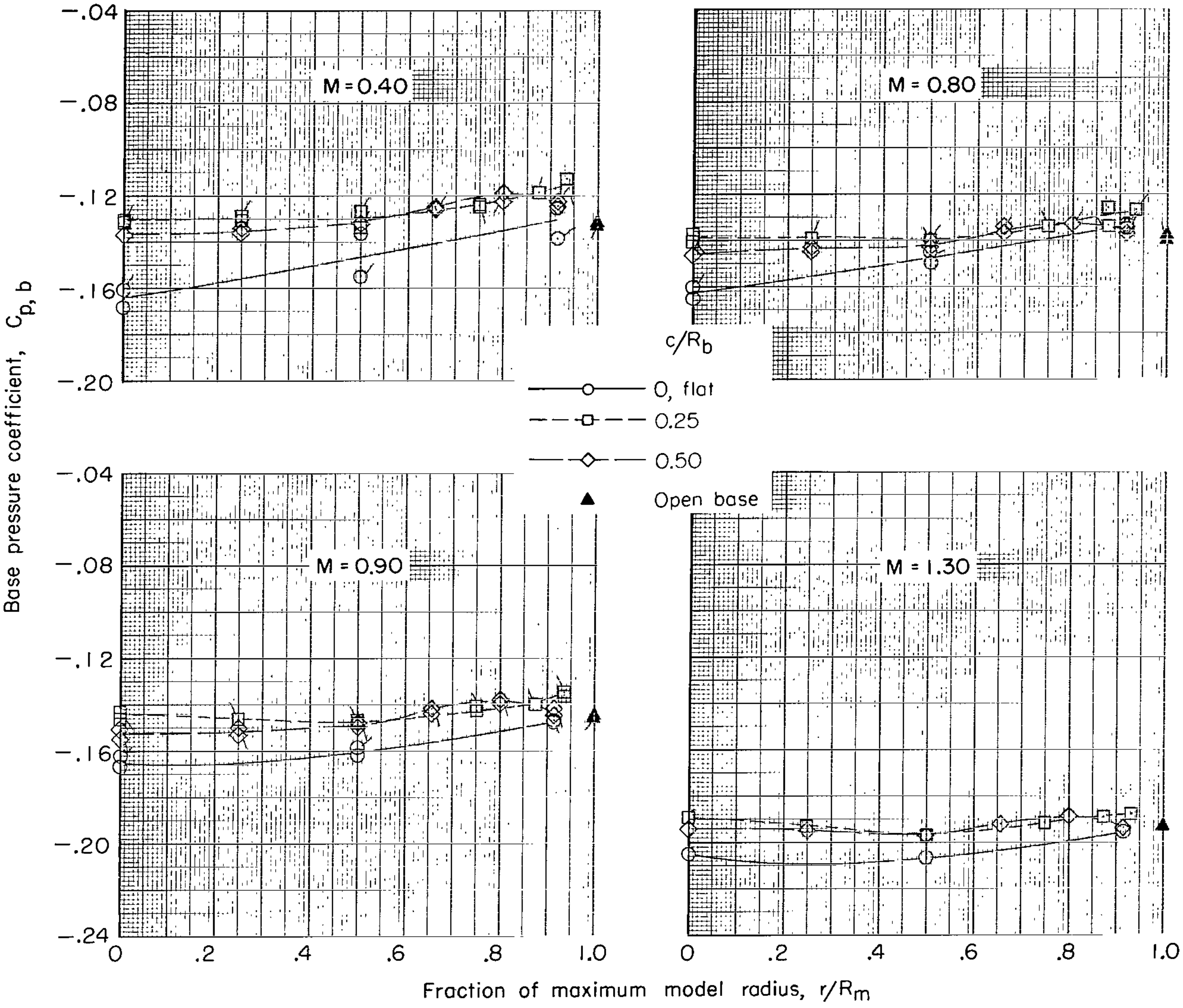

(d) $L/D_m = 1.5$; $\beta = 0^0$; $A_b/A_m = 1.00$.

Figure 14.- Continued.

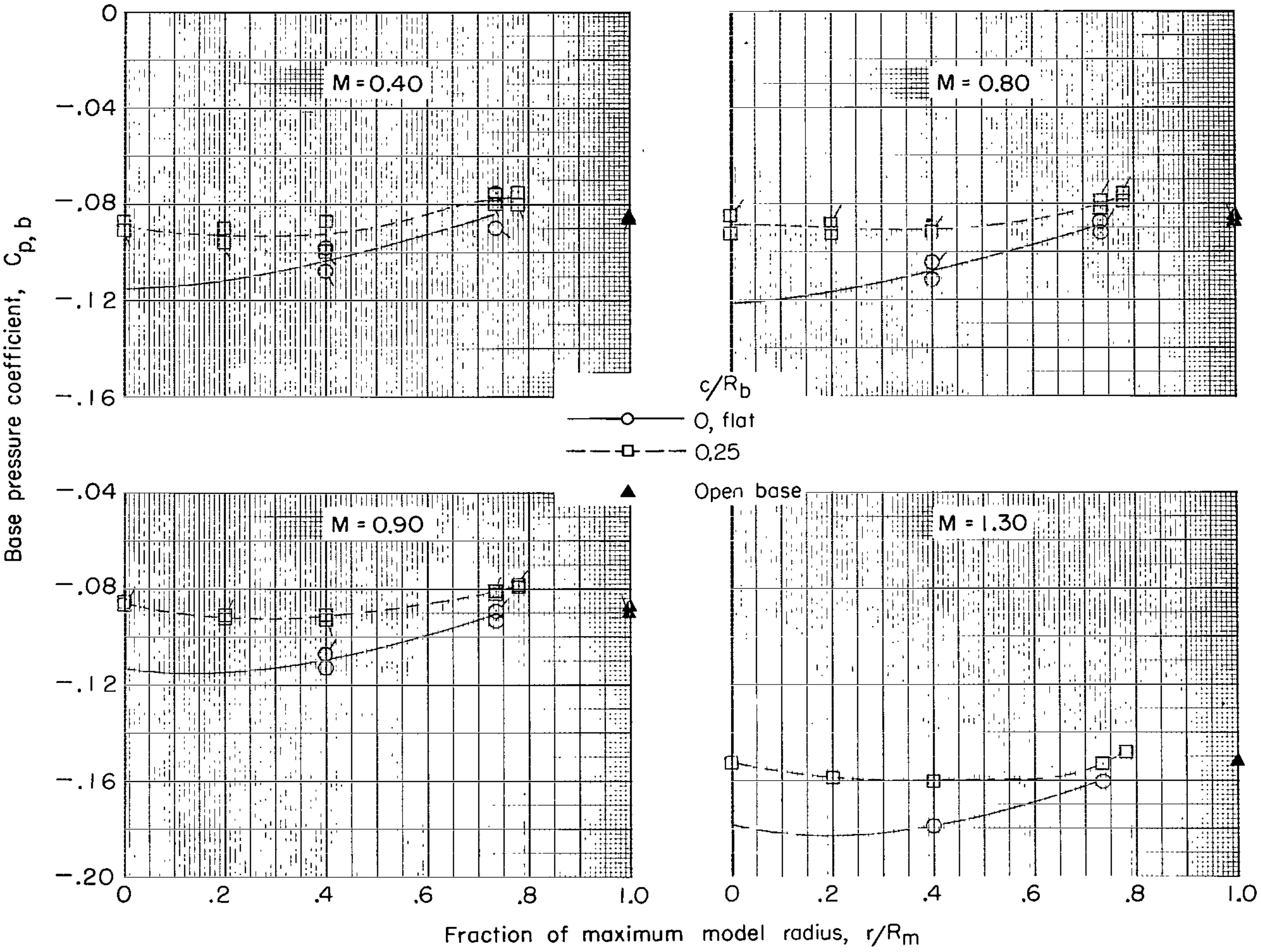

(e) $L/D_m = 1.5$; $\beta = 3^{\circ}$; $A_b/A_m = 0.70$.

Figure 14.- Continued.

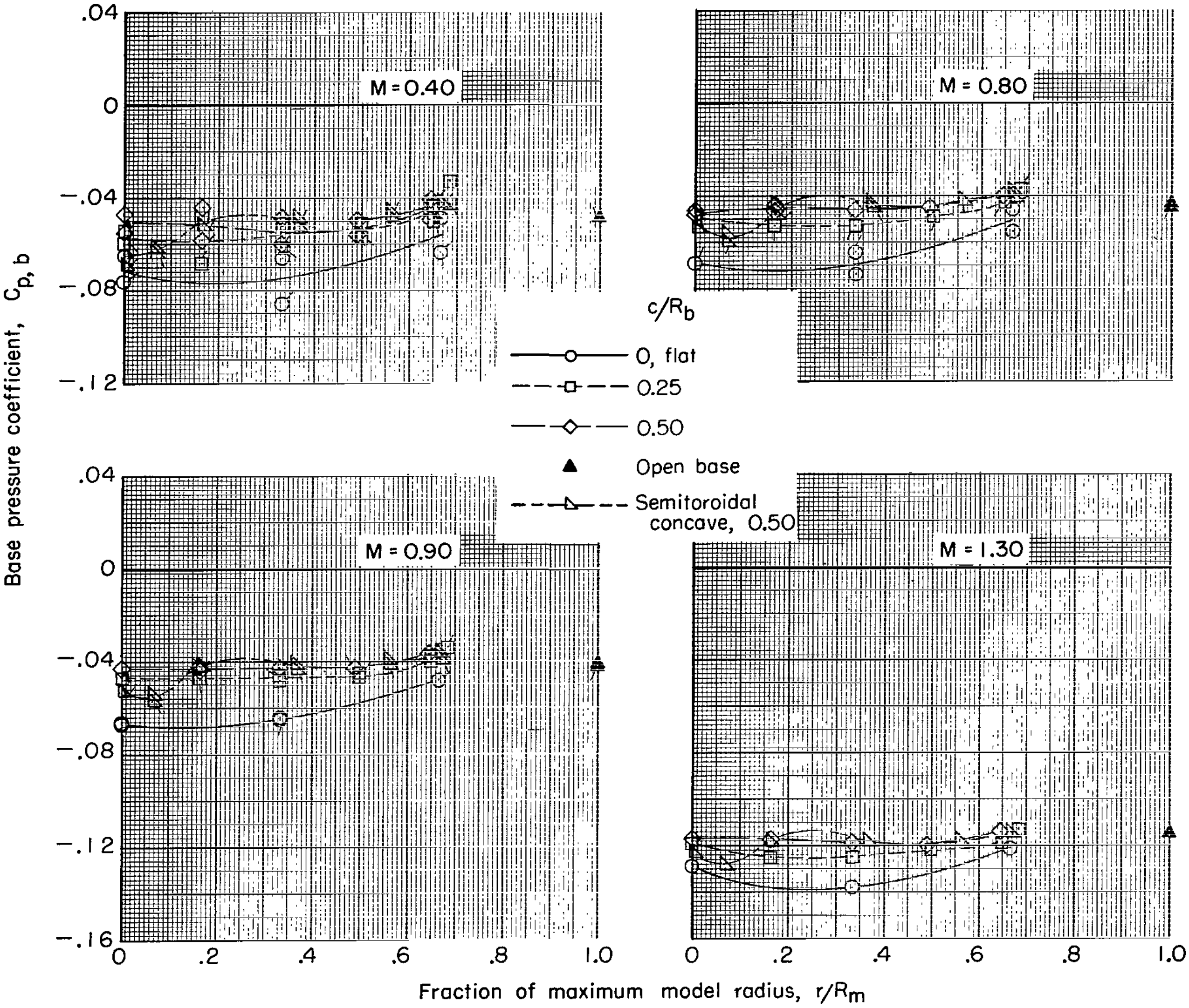

(f) $L/D_m = 1.5$; $\beta = 5^{\circ}$; $A_b/A_m = 0.55$.

Figure 14.- Continued.

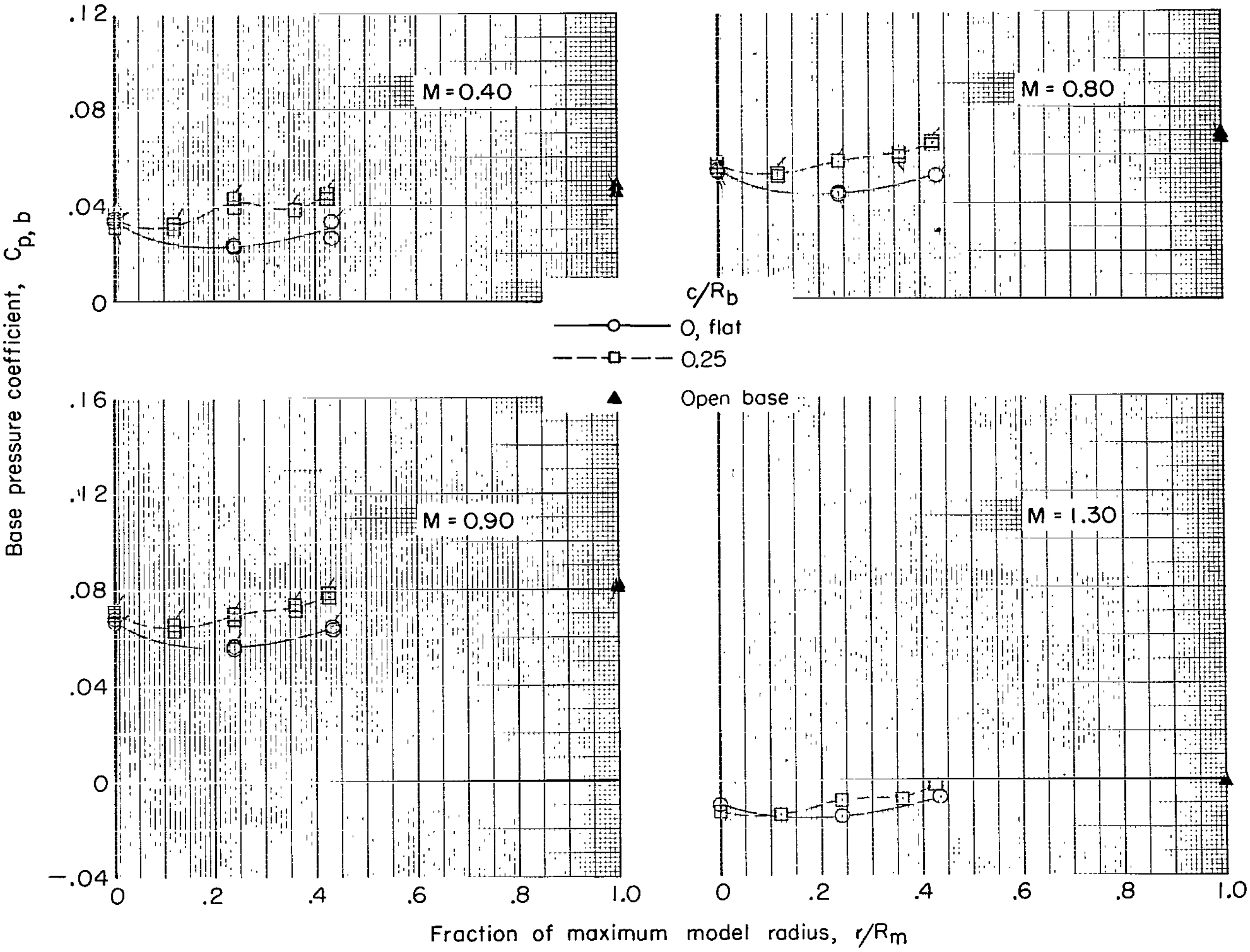

(g) $L/D_m = 1.5$; $\beta = 10^0$; $A_b/A_m = 0.23$.

Figure 14.- Concluded.

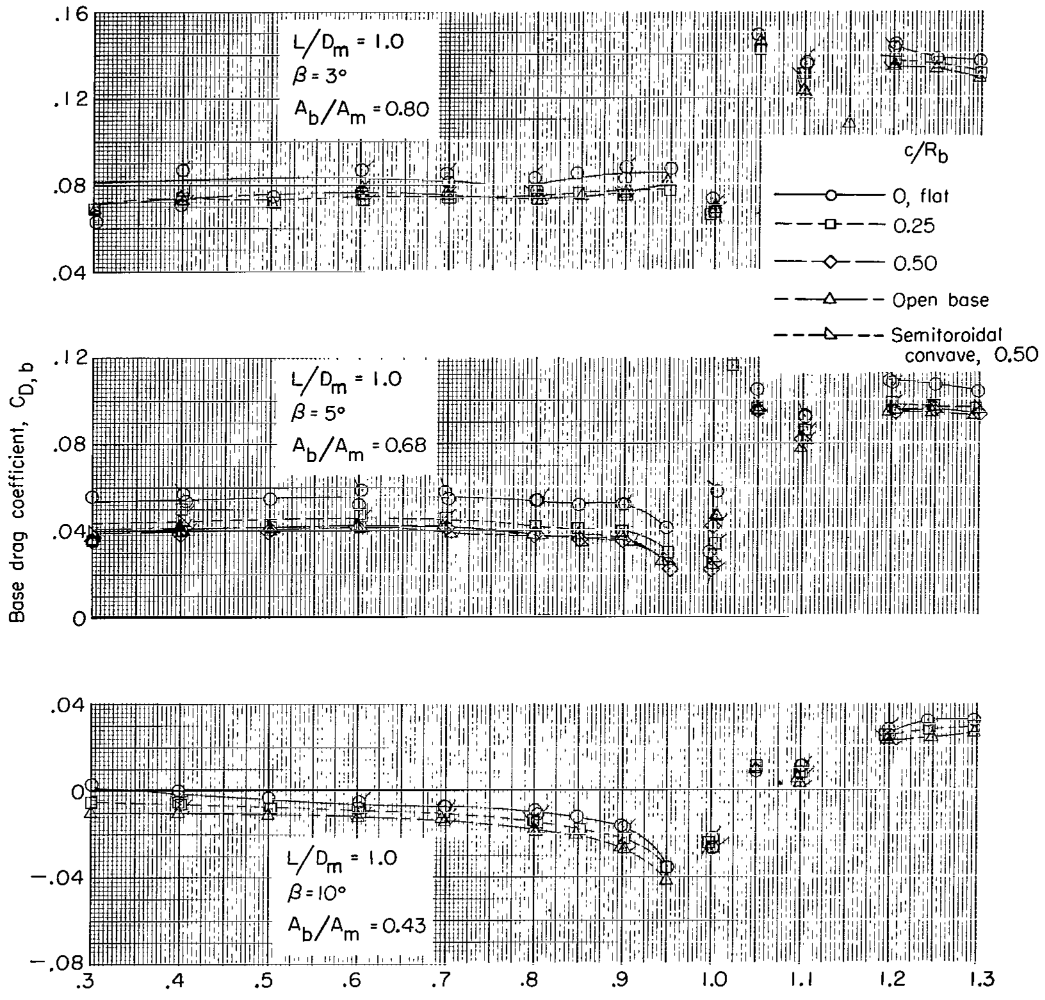

(a) $L/D_m = 1.0$.

Figure 15.- Base drag coefficient as a function of free-stream Mach number for various configurations, with orifice rows at $\Phi = 0^{\circ}$. (Flagged symbols indicate data taken as Mach number was decreased.)

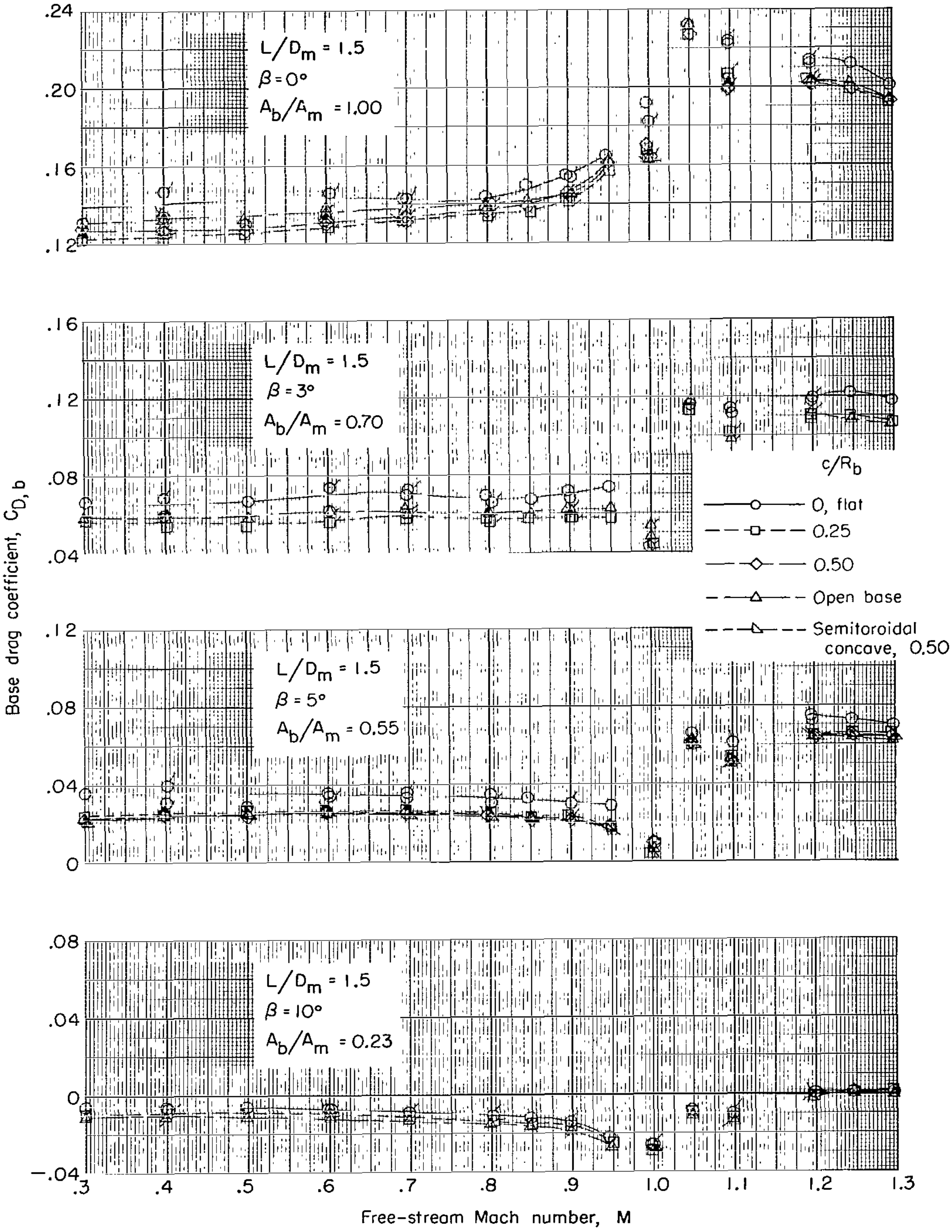

(b) $L/D_m = 1.5$.

Figure 15.- Concluded.

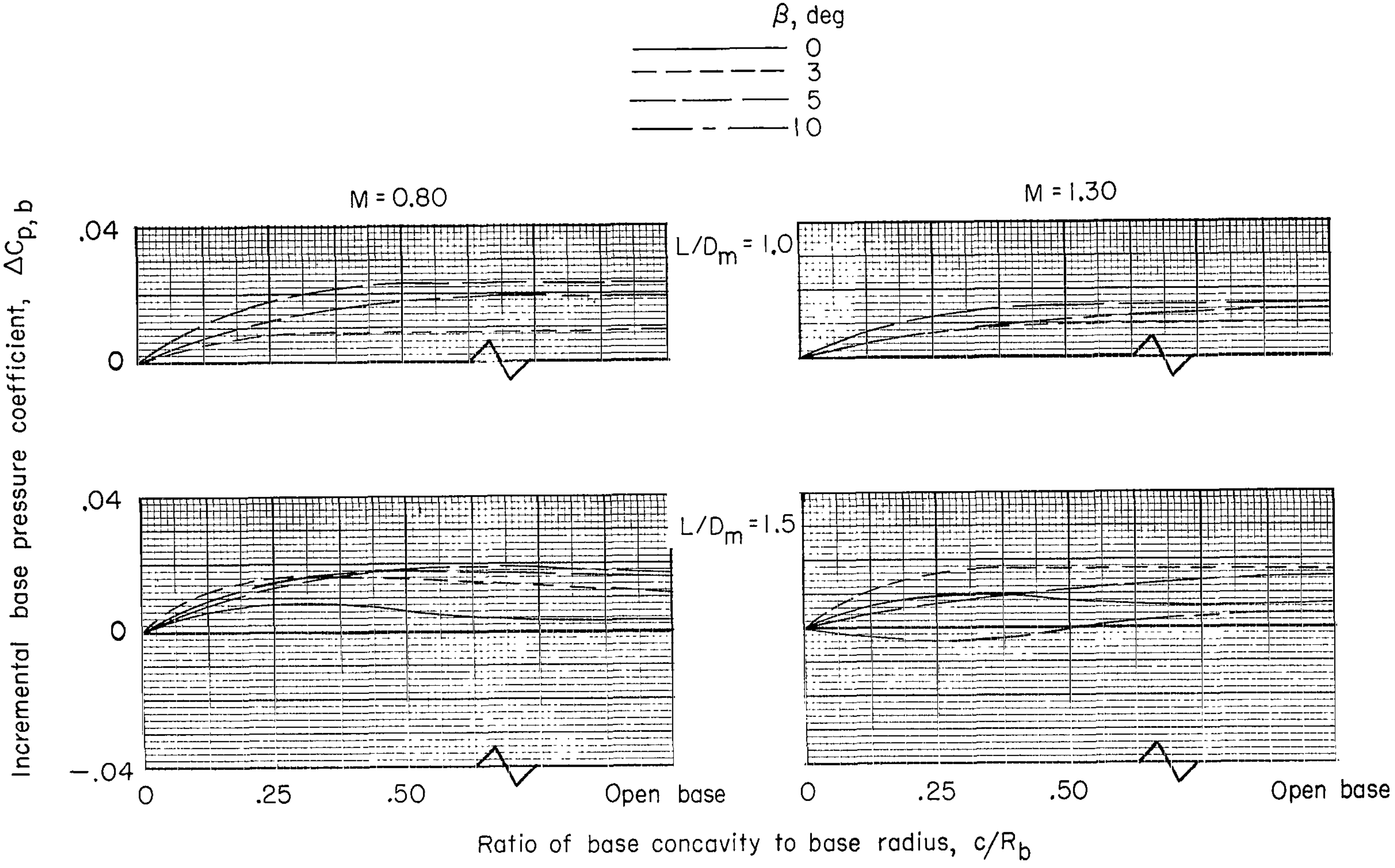

Figure 16.- Change in base pressure coefficient derived from concaving the base as a function of ratio of base concavity to base radius for several boattail angles and for both boattail lengths at Mach numbers of 0.80 and 1.30.

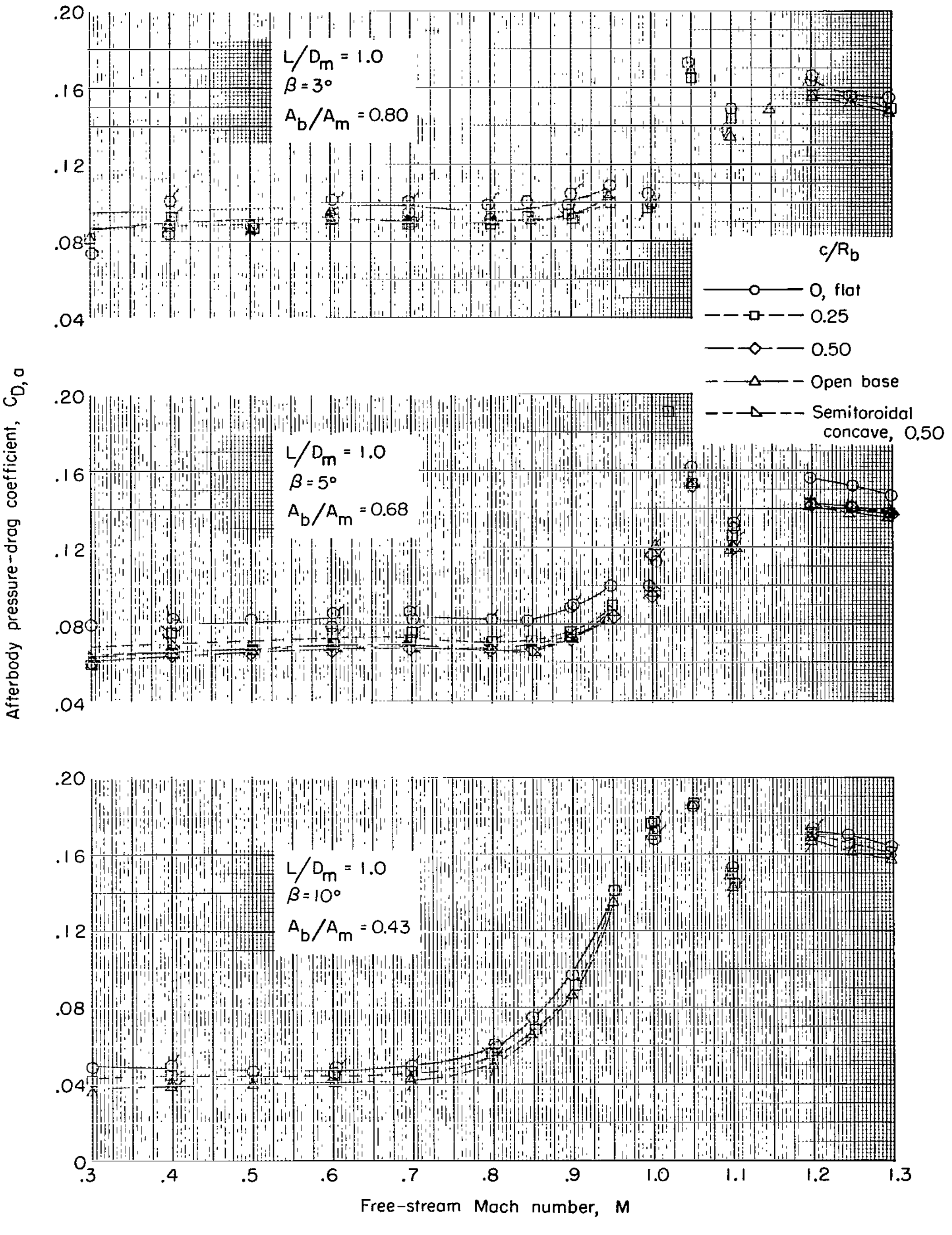

(a) $L/D_m = 1.0$.

Figure 17.- Afterbody pressure-drag coefficient as a function of free-stream Mach number for various configurations, with orifice rows at $\Phi = 0^{\circ}$. (Flagged symbols indicate data taken as Mach number was decreased.)

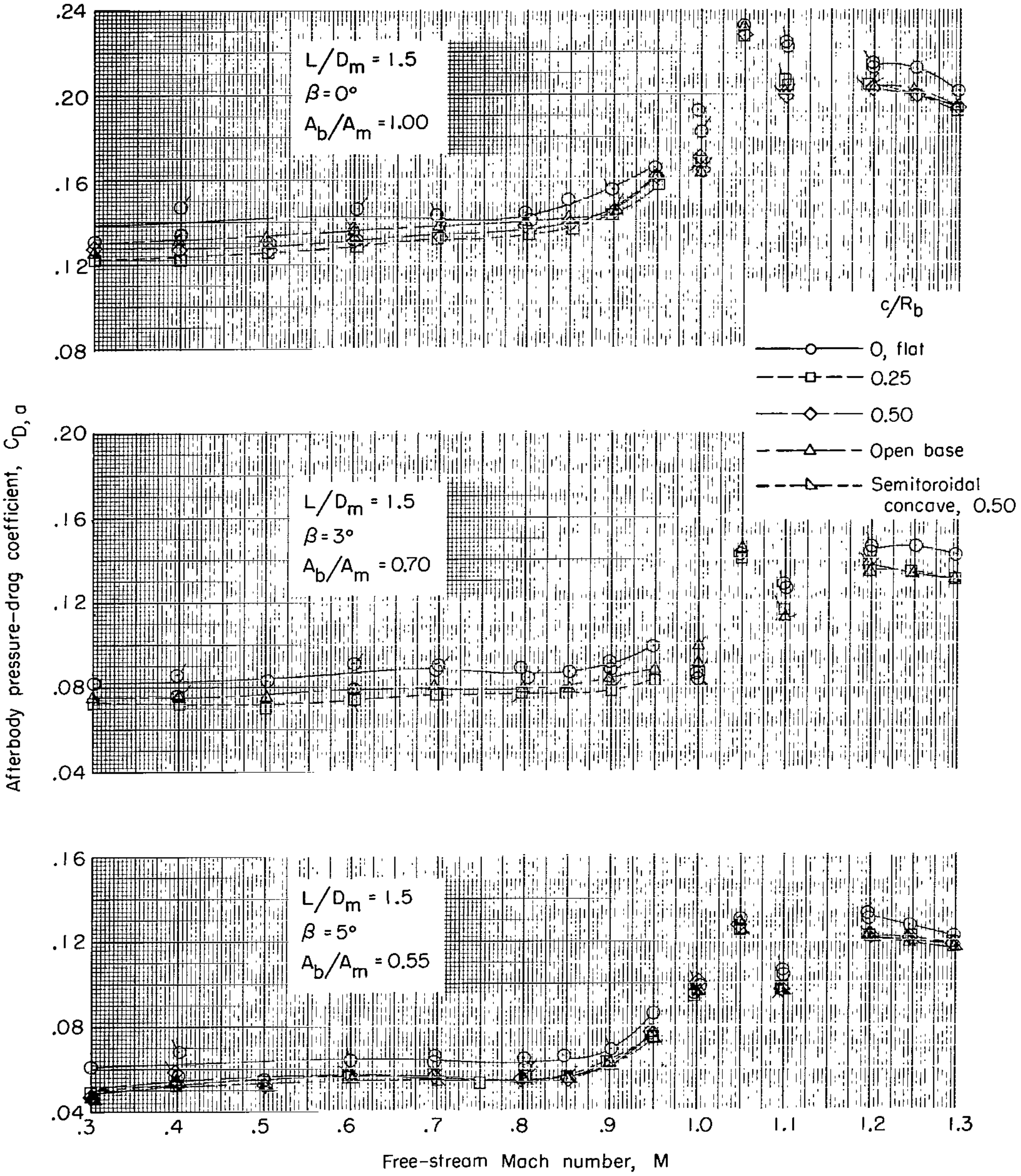

(b) $L/D_m = 1.5$; $\beta = 0^0$, 3^0, and 5^0.

Figure 17.- Continued.

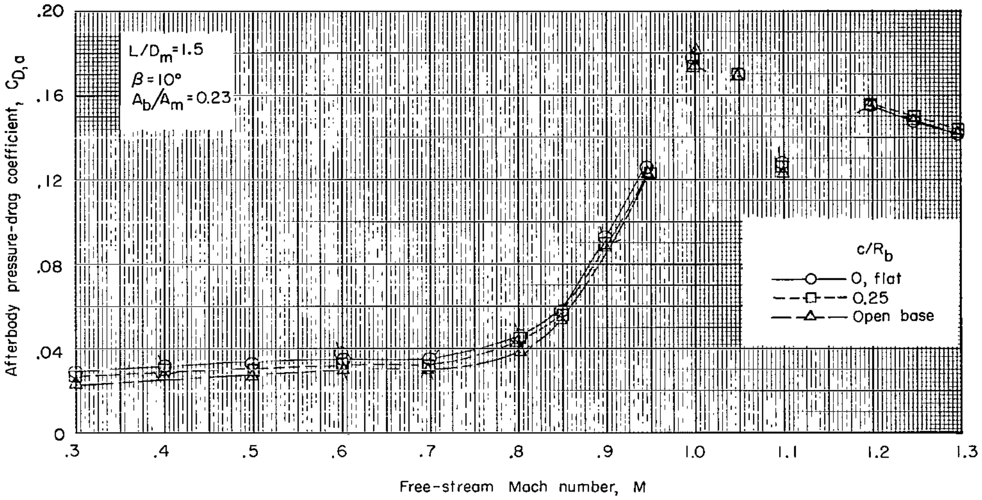

(c) $L/D_m = 1.5$; $\beta = 10^0$.

Figure 17.- Concluded.

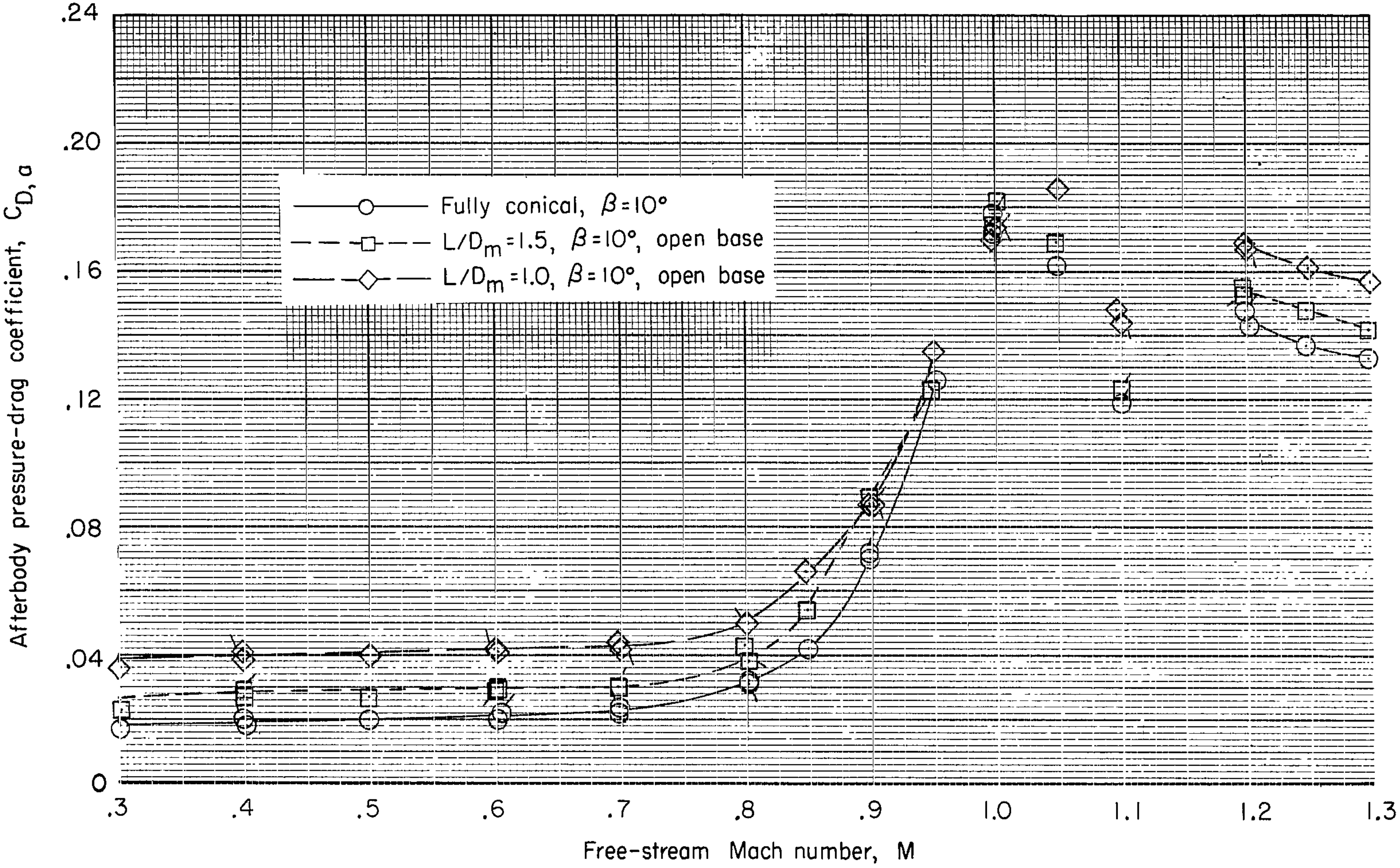

Figure 18.- Afterbody pressure-drag coefficient as a function of free-stream Mach number for afterbodies with boattail angles of 10^0 and with orifice rows at Φ = 0^0.

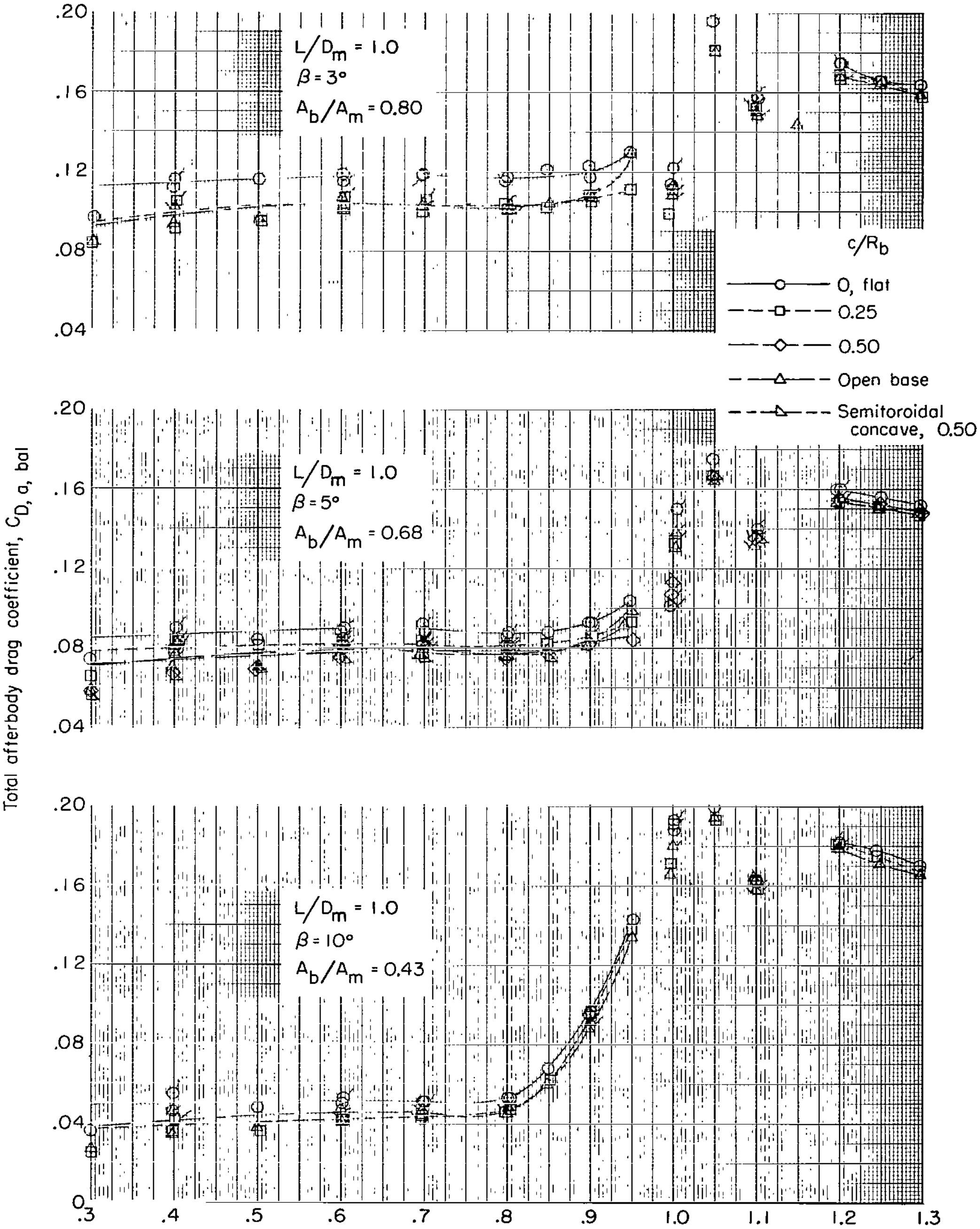

(a) $L/D_m = 1.0$.

Figure 19.- Total afterbody drag coefficient as a function of free-stream Mach number for various configurations. (Flagged symbols indicate data taken as Mach number was decreased.)

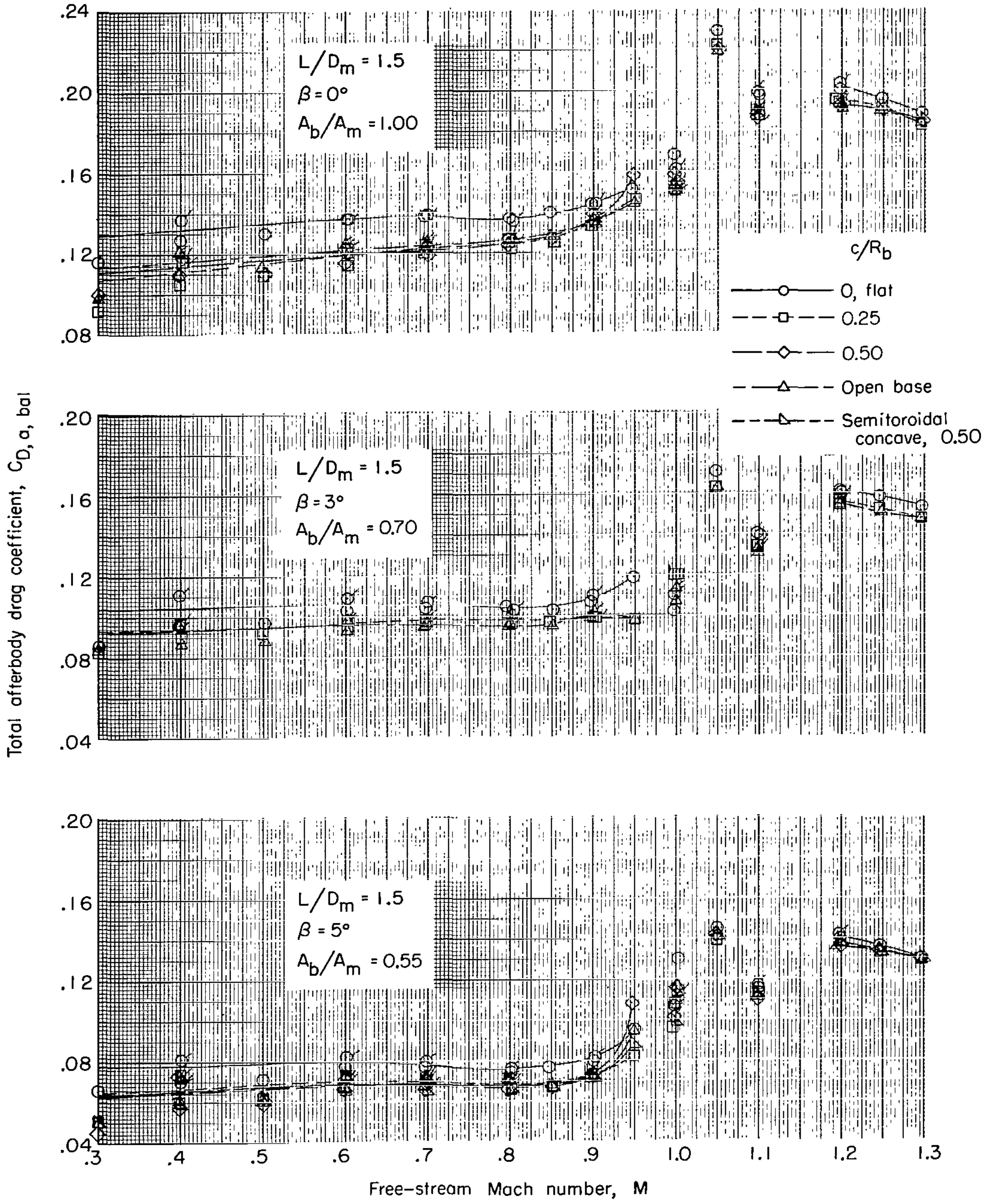

(b) $L/D_m = 1.5$; $\beta = 0^{0}$; 3^{0}, and 5^{0}.

Figure 19.- Continued.

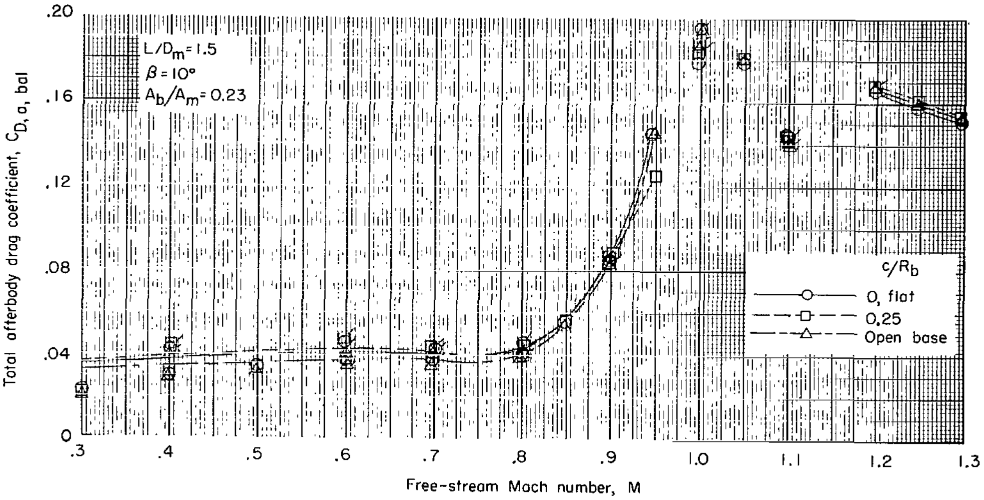

(c) $L/D_m = 1.5$; $\beta = 10^0$.

Figure 19.- Concluded.

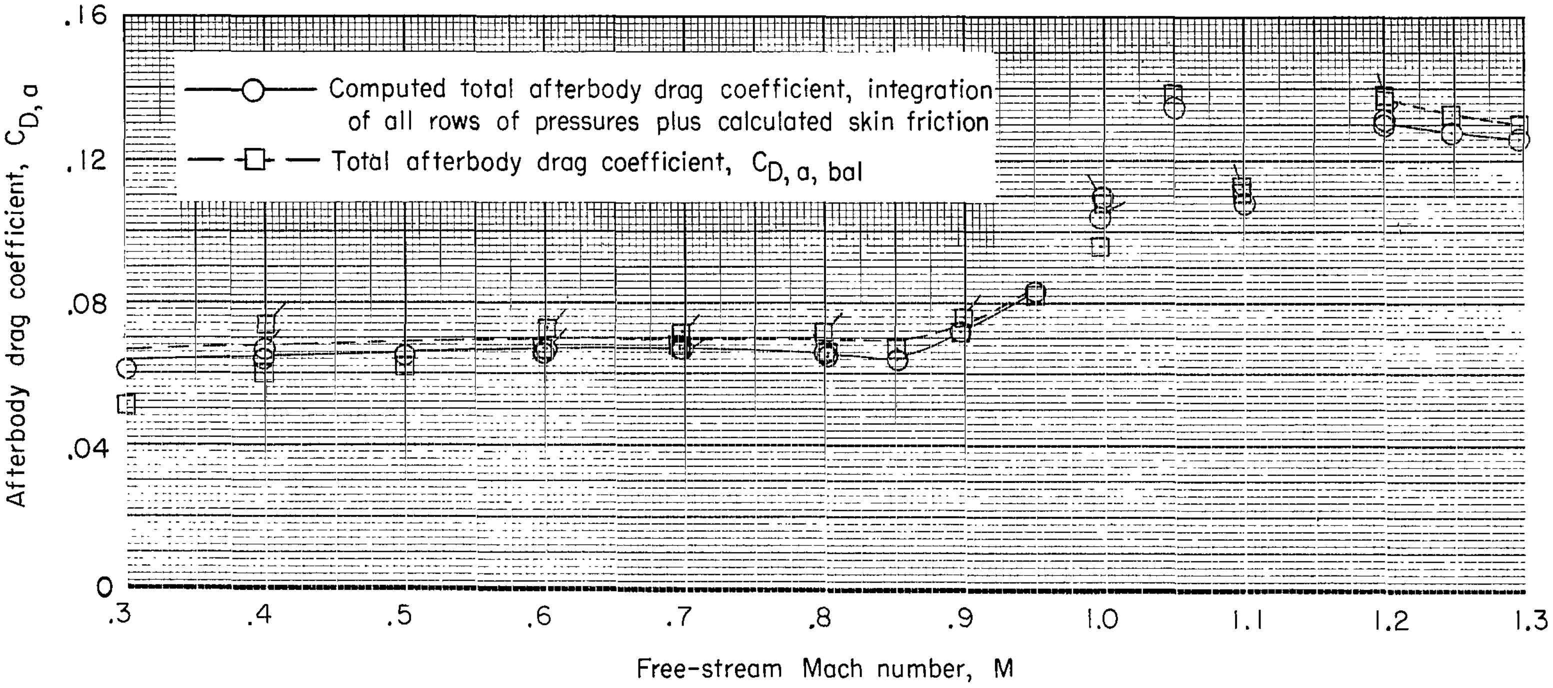

Figure 20.- Afterbody drag coefficient as a function of free-stream Mach number for calculated pressure and balance drags. $L/D_m = 1.5$; $\beta = 5^0$; concave base $\left(c/R_b \approx 0.25\right)$. (Flagged symbols indicate data taken as Mach number was decreased.)

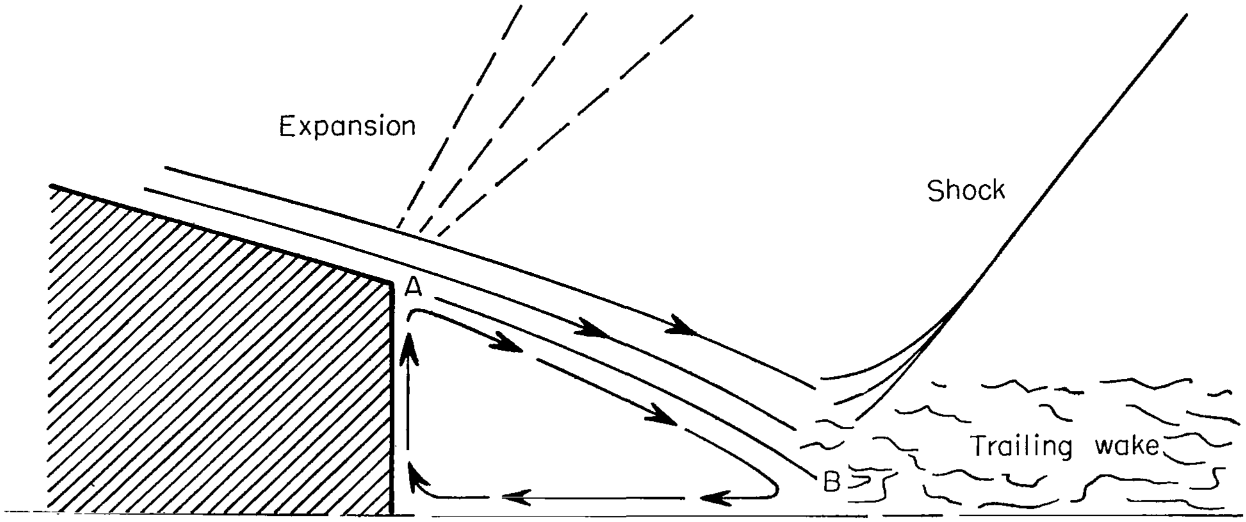

(a) Flat base.

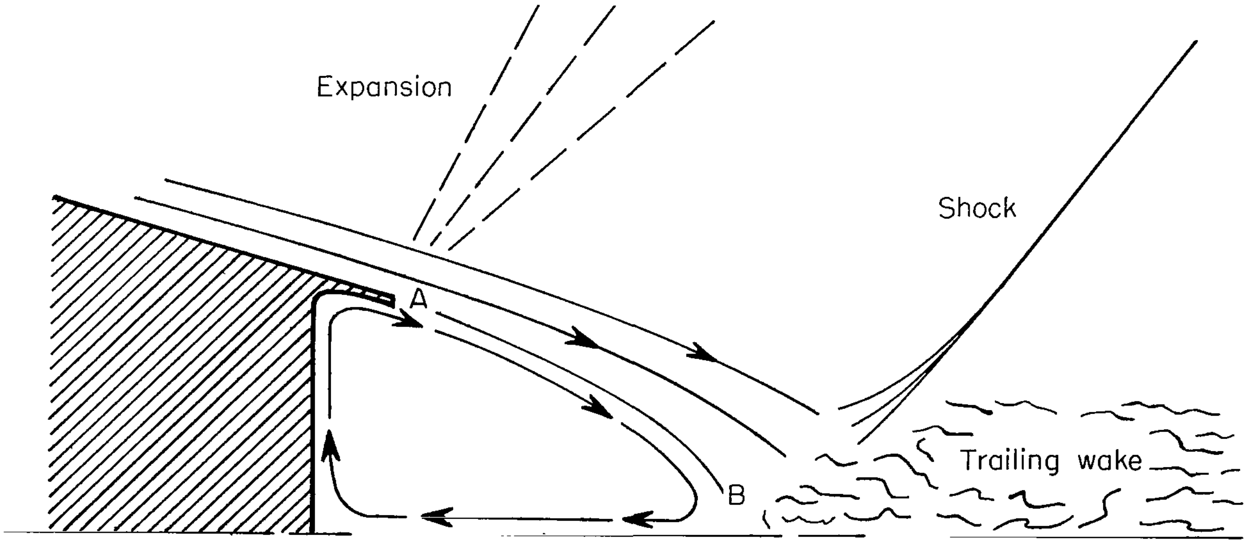

(b) Concave base.

Figure 21.- Graphical illustration of axisymmetric flow at base in a viscous supersonic stream.

NATIONAL AERONAUTICS AND SPACE ADMINISTRATION
WASHINGTON, D.C. 20546

OFFICIAL BUSINESS

FIRST CLASS MAIL

POSTAGE AND FEES PAID
NATIONAL AERONAUTICS AND
SPACE ADMINISTRATION

020 001 26 51 3DS 68285 00903
AIR FORCE WEAPONS LABORATORY/AFWL/
KIRTLAND AIR FORCE BASE, NEW MEXICO 8711

ATT E. LOU BOWMAN, ACTING CHIEF TECH. LI

POSTMASTER: If Undeliverable (Section 158 Postal Manual) Do Not Return

> *"The aeronautical and space activities of the United States shall be conducted so as to contribute . . . to the expansion of human knowledge of phenomena in the atmosphere and space. The Administration shall provide for the widest practicable and appropriate dissemination of information concerning its activities and the results thereof."*
>
> —NATIONAL AERONAUTICS AND SPACE ACT OF 1958

NASA SCIENTIFIC AND TECHNICAL PUBLICATIONS

TECHNICAL REPORTS: Scientific and technical information considered important, complete, and a lasting contribution to existing knowledge.

TECHNICAL NOTES: Information less broad in scope but nevertheless of importance as a contribution to existing knowledge.

TECHNICAL MEMORANDUMS: Information receiving limited distribution because of preliminary data, security classification, or other reasons.

CONTRACTOR REPORTS: Scientific and technical information generated under a NASA contract or grant and considered an important contribution to existing knowledge.

TECHNICAL TRANSLATIONS: Information published in a foreign language considered to merit NASA distribution in English.

SPECIAL PUBLICATIONS: Information derived from or of value to NASA activities. Publications include conference proceedings, monographs, data compilations, handbooks, sourcebooks, and special bibliographies.

TECHNOLOGY UTILIZATION PUBLICATIONS: Information on technology used by NASA that may be of particular interest in commercial and other non-aerospace applications. Publications include Tech Briefs, Technology Utilization Reports and Notes, and Technology Surveys.

Details on the availability of these publications may be obtained from:

SCIENTIFIC AND TECHNICAL INFORMATION DIVISION
NATIONAL AERONAUTICS AND SPACE ADMINISTRATION
Washington, D.C. 20546